

# Dynamic splitting tensile behaviour of engineered geopolymer composites with hybrid polyvinyl alcohol and recycled tyre polymer fibres

Hui Zhong, Mingzhong Zhang\*

*Department of Civil, Environmental and Geomatic Engineering, University College London,  
London, WC1E 6BT, UK*

**Abstract:** Partial replacement of the widely used polyvinyl alcohol (PVA) fibre in engineered geopolymer composites (EGC) with recycled fibres can reduce the material cost and improve sustainability. This study investigates the effect of hybrid PVA and recycled tyre polymer (RTP) fibre content on the quasi-static and dynamic splitting tensile behaviour and microstructure of ambient-cured fly ash-slag based EGC through split Hopkinson pressure bar, scanning electron microscopy and X-ray computed tomography tests. Results indicate that the presence of PVA or RTP fibres can considerably improve the quasi-static and dynamic splitting tensile behaviour of geopolymers. All investigated mixtures are characterised by remarkable strain rate sensitivity within the considered test range, which can be well described using the proposed relationship between dynamic increase factor and strain rate for predictions of dynamic properties. Replacing PVA fibre with 0.25-0.5% RTP fibre can lead to better dynamic splitting tensile properties of EGC compared to that with 2.0% PVA fibre, which can be mainly ascribed to the improved synergistic effect of hybrid fibres in controlling the cracks. The microscopic images reveal that the failure mode of RTP fibres is not sensitive to the strain rate due to its hydrophobic surface feature, which could benefit the energy absorption capacity of EGC under dynamic loading. EGC containing hybrid PVA and RTP fibres holds promise as a cost-effective and sustainable material for applications against dynamic loadings.

**Keywords:** Alkali-activated concrete; Hybrid fibre reinforced concrete; Split Hopkinson pressure bar; Dynamic increase factor; Microstructure

## 1. Introduction

Engineered geopolymer composite (EGC) has emerged recently as a promising substitute for engineered cementitious composite (ECC) because of its enhanced sustainability. The replacement of cementitious matrix with cement-free geopolymer matrix can reduce carbon emission and energy consumption by about 60-70% ([Davidovits, 2002](#)). Similar to ECC, EGC can be tailored through micromechanics-based design to exhibit strain-hardening and multiple cracking behaviour under tensile loading ([Li, 2019](#); [Lyu et al., 2021](#)), which can typically possess a tensile strength of 3.4-5.8 MPa, a tensile strain capacity of 2.3-5.8% and an average crack width of 28.4-147.3  $\mu\text{m}$  at 28 d (for fly ash-slag based EGC) ([Kan et al., 2021](#); [Nematollahi et al., 2017a, b](#); [Wang et al., 2022](#); [Zhang, S. et al., 2020](#); [Zhong and Zhang, 2021](#)). Given the superior tensile behaviour, EGC is promising to be

---

\* Corresponding author. E-mail address: mingzhong.zhang@ucl.ac.uk (M. Zhang)

applied in various applications such as high-rise buildings and 3D concrete printing ([Maruta, 2005](#); [Zhong and Zhang, 2022a](#)).

So far, different types of EGC have been developed with various precursors, alkaline activators, aggregates and fibres. Among them, fly ash, ground granulated blast-furnace slag and their blends are the commonly used precursors for EGC due to their large quantities around the world and relatively stable chemical components ([Duxson et al., 2007](#); [Zhang et al., 2021](#)). Recently, EGC made of blended fly ash and slag has received an increasing attention as it can not only overcome some limitations existing in fly ash-based EGC (e.g., requirement of heat curing for early strength) and slag-based EGC (e.g., low workability, rapid setting and high shrinkage) but can also possess superior engineering properties under ambient temperature ([Nematollahi et al., 2017a, b](#); [Wang et al., 2020](#); [Wang et al., 2021](#); [Wang et al., 2022](#); [Zhang, S. et al., 2020](#); [Zhong and Zhang, 2021](#)). Sodium-based alkaline activators (e.g., sodium hydroxide and sodium silicate) in either liquid ([Farooq et al., 2022](#); [Zhong and Zhang, 2021](#)) or solid ([Nematollahi et al., 2017a, b](#)) state are often used to produce EGC. Like ECC, micro silica sand is generally adopted as fine aggregate for EGC and coarse aggregate is normally prohibited as it can increase the fracture toughness of the matrix and thus weaken the strain-hardening and multiple cracking features of EGC ([Khan et al., 2016](#)). Hydrophilic polyvinyl alcohol (PVA) fibres with oil coating are mainly used at a fibre volume fraction of no higher than 2.0% to achieve the desired ductility for EGC ([Nematollahi et al., 2014](#); [Nguyễn et al., 2021](#)). Hydrophobic polyethylene (PE) fibres with a tensile strength of 2700-3500 MPa are also adopted as reinforcement to develop EGC that has high strength and superior ductility ([Lee et al., 2017](#); [Nematollahi et al., 2017a](#); [Zhao et al., 2021](#)). Nevertheless, the exceptionally high costs and inevitable environmental impacts during the production of these fibres would impede the large-scale application and sustainable development of EGC ([Merli et al., 2019](#); [Yu and Leung, 2017](#); [Zhang, D. et al., 2020](#)). It was reported that the cost of PVA fibre accounts for approximately 54-70% of the total material cost of EGC ([Zhong and Zhang, 2021](#)), and the production of PVA fibre consumes fossil fuels, leading to high embodied carbon and embodied energy ([Van den Heede et al., 2018](#)). Therefore, it is vital to find fibres with lower cost and higher sustainability as alternatives to PVA or PE fibres in EGC.

In recent years, an increasing number of studies have focused on the use of recycled fibres from wastes to replace PVA or PE fibres in either ECC or EGC, which can not only improve the cost-effectiveness and sustainability of ECC or EGC but also reduce the amount of solid wastes. It was found that using recycled polyethylene terephthalate (PET) fibres from waste plastic bottles to replace 50% of PVA fibre in ECC can reduce the material cost and embodied energy by around 20-40% without obviously weakening the uniaxial tensile behaviour especially strain-hardening and multiple cracking behaviour ([Yu et al., 2018](#)). In addition, ECC with hybrid PVA and recycled PET fibres can exhibit excellent impact resistance with adequate tensile performance ([Lu et al., 2018b](#)). The previous

studies ([Wang et al., 2020](#); [Zhong and Zhang, 2021](#)) on the feasibility of using recycled tyre fibres to partially replace PVA fibres in EGC indicate that by replacing PVA fibre with 0.25-0.5% (by volume) recycled tyre steel fibre, the compressive strength and drying shrinkage resistance of EGC were about 14-26% and 62-73% higher than those of EGC with 2.0% PVA fibre. Apart from recycled tyre steel fibres, another major output from the recycling of waste tyre called recycled tyre polymer (RTP) fibre was found to be feasible to substitute PVA fibre in EGC to reduce the material cost and embodied energy while maintaining acceptable engineering properties. These studies have only focused on the static mechanical properties of EGC with recycled fibres, while the dynamic behaviour has been rarely investigated. The presence of a certain content of RTP fibres can improve the mechanical properties of EGC under dynamic compression ([Zhong and Zhang, 2022b](#)), while the dynamic tensile behaviour of EGC containing RTP fibres remains unclear, which would hinder its widespread application as concrete structures may fail more easily in tension when subjected to dynamic loadings, e.g., earthquake and explosive blast ([Malvar and Ross, 1998](#); [Yoo and Banthia, 2019](#)).

Up to now, to the authors' best knowledge, only two studies ([Farooq et al., 2022](#); [Trindade et al., 2020](#)) have explored the dynamic tensile behaviour of EGC with PVA or PE fibres using the direct tension approach, i.e., direct tensile and split Hopkinson tension bar tests. Independent of the curing regime (ambient or heat curing), the tensile strength of all EGC mixtures under dynamic loading was higher than that under quasi-static loading, and all heat-cured EGC exhibited ductile failure mode, although heat curing impaired the compressive and tensile strengths of EGC ([Farooq et al., 2022](#)). Moreover, fly ash-slag based EGC outperformed fly ash-based and slag-based EGC in terms of quasi-static and dynamic tensile properties. In comparison with PVA fibre reinforced EGC, PE fibre reinforced EGC yielded better dynamic tensile strain capacity, dynamic bond strength and energy absorption capacity ([Trindade et al., 2020](#)). Besides, it had better dynamic tensile performance than ECC reinforced with the same fibre due to the comparable matrix stiffness and crack-bridging stiffness. It was indicated that the tensile behaviour of EGC is sensitive to strain rate, while only limited strain rates including  $0.51 \text{ s}^{-1}$  ([Farooq et al., 2022](#)) and  $300\text{-}330 \text{ s}^{-1}$  ([Trindade et al., 2020](#)) were considered in these studies, which is not sufficient to understand its tensile performance when subjected to various dynamic loadings. In addition, compared to the direct tension method, employing an indirect tension, i.e., dynamic splitting tensile test using a split Hopkinson pressure bar (SHPB), to investigate the tensile behaviour of EGC has several advantages. For instance, the test setup and sample preparation are simpler ([Khan et al., 2019](#)), and more reliable results can be obtained because of better achievement of stress equilibrium whilst dynamic loading via pulse shaping technique ([Chen et al., 2014](#)). Given these benefits, a rising number of studies have adopted the indirect approach to explore the dynamic tensile behaviour of fibre reinforced composites ([Khan et al., 2019](#); [Lai et al., 2022](#); [Zhao et al., 2020](#)). To ensure the safe design of structural members made from EGC containing

RTP fibres, it is vital to comprehensively investigate the effects of various strain rates and fibre contents on the dynamic tensile behaviour of EGC using the indirect tension approach.

The main purpose of this study is to investigate the dynamic splitting tensile behaviour of ambient-cured fly ash-slag based EGC reinforced with hybrid PVA fibre (1.0-2.0%) and RTP fibre (0-1.0%) at various strain rates ( $10^{-1} \text{ s}^{-1}$  to  $10^1 \text{ s}^{-1}$ ). Firstly, the quasi-static splitting tensile strength of all studied mixtures was measured, which is an important parameter for deriving the dynamic increase factor (DIF) that denotes the ratio of dynamic splitting tensile strength to quasi-static splitting tensile strength. Then, the dynamic splitting tensile behaviour in terms of failure pattern, stress-displacement curve, dynamic splitting tensile strength, DIF and energy absorption capacity were explored using SHPB. Based on the experimental data obtained, some empirical equations were proposed to estimate the relationships between DIF and strain rate. Lastly, a series of microstructural characterisations were conducted to detect the fibre conditions after static and dynamic splitting tension and gain insight into the underlying mechanisms of the synergistic effect of hybrid fibres as compared to mono-PVA fibre reinforced EGC in terms of quasi-static and dynamic mechanical properties, material cost and sustainability.

## 2. Experimental program

### 2.1. Raw materials

In this study, low-calcium fly ash and ground granulated blast-furnace slag were used as precursors, the chemical composition and particle size distribution of which are presented in [Table 1](#) and [Fig. 1](#), respectively. Silica sand with a maximum particle size of 250  $\mu\text{m}$  was used as aggregate. The alkaline activator was prepared by blending sodium hydroxide solution (molarity: 10 M) and sodium silicate solution (silicate modulus: 3.15). Polycarboxylate-based superplasticiser was utilised to improve the flowability of mixtures. The geopolymer matrix was either reinforced with mono-PVA fibres or hybrid PVA and RTP fibres ([Fig. 2](#)). [Table 2](#) summarises the main properties of PVA and RTP fibres. The properties of PVA fibres were provided by the manufacturer (Kuraray Co., Ltd., Japan) while that of RTP fibres was characterised by the authors. The detailed characterisation process can be found in a previous study ([Zhong and Zhang, 2021](#)). The thermal behaviour of RTP fibres was studied using a simultaneous thermal analyser (NETZSCH STA 409 PC/PG) at a constant heating rate of 10  $^{\circ}\text{C}/\text{min}$  from 30-800  $^{\circ}\text{C}$  under nitrogen flow rate (100 mL/min). The thermogravimetric analysis (TGA) and differential scanning calorimetry (DSC) results are shown in [Fig. 3](#). The melting point of RTP fibres was about 254  $^{\circ}\text{C}$  and they started to decompose at around 409  $^{\circ}\text{C}$ , suggesting that RTP fibres had similar thermal behaviour to that of PET fibre and the main composition of RTP fibres was PET ([Zhang and Tan, 2020](#)).

**Table 1** Chemical compositions (wt.%) of fly ash and ground granulated blast-furnace slag.

Oxide	SiO <sub>2</sub>	Al <sub>2</sub> O <sub>3</sub>	Fe <sub>2</sub> O <sub>3</sub>	CaO	SO <sub>3</sub>	MgO	TiO <sub>2</sub>	P <sub>2</sub> O <sub>5</sub>	Loss on Ignition
Fly ash	57.02	32.35	3.01	2.88	0.41	0.58	1.26	0.20	2.45
Slag	31.85	17.31	0.34	41.20	1.78	6.13	0.62	0.02	0.39

**Table 2** Properties of polyvinyl alcohol (PVA) and recycled tyre polymer (RTP) fibres.

Fibre	Length (mm)	Diameter (µm)	Tensile strength (MPa)	Elastic modulus (Ga)	Density (kg/m <sup>3</sup> )
PVA	12	40	1560	41	1300
RTP	5.2 (2.4)	21.4 (4.4)	761 (115)	3.8 (0.7)	1476 (3)

Note: the values are standard deviations in parentheses.

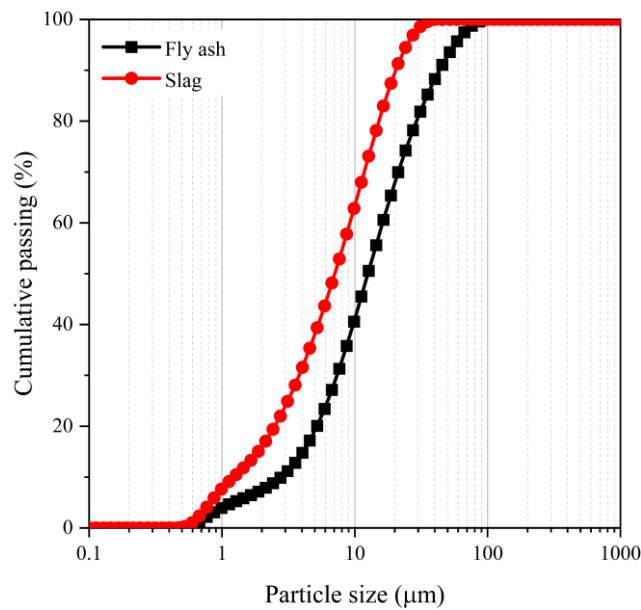


**Fig. 1.** Particle size distribution of fly ash and ground granulated blast-furnace slag.

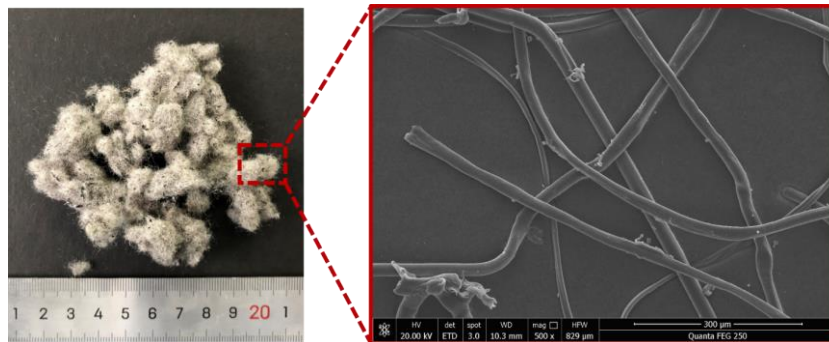


**Fig. 2.** Photograph and SEM image of RTP fibres.

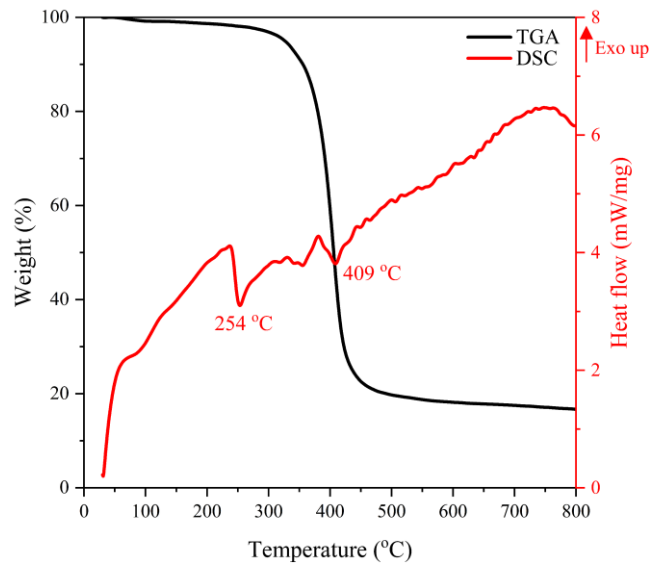


**Fig. 3.** Thermogravimetric analysis (TGA) and differential scanning calorimetry (DSC) results of RTP fibres.

## 2.2. Mix proportions

Based on a previous study ([Zhong and Zhang, 2021](#)), replacing PVA fibres with RTP fibres in EGC can lead to higher drying shrinkage resistance, cost-effectiveness and sustainability but poorer quasi-static tensile properties, compared to EGC with 2.0% PVA fibre. It is worth noting that utilising a small dosage of RTP fibre (e.g., 0.25%) can achieve pronounced strain-hardening and multiple cracking behaviour for EGC, which was comparable with EGC reinforced with 2.0% PVA fibre. In this study, the variables were kept consistent with our previous study, which included fibre type and fibre content. The upper limit of RTP fibre volume fraction was set as 1.0% as it would be challenging for EGC to exhibit strain-hardening and multiple cracking behaviour if the incorporated PVA fibre dosage is less than 1.0% and the overall properties of composites can be significantly reduced when more than 1.0% RTP fibre content is added ([Chen et al., 2019](#); [Yu et al., 2018](#)). **Table 3** shows the mix proportions for different mix IDs. Regarding the meaning of the mix ID, for instance, 1.5P-0.5R denotes that the mixture contained 1.5% PVA fibre and 0.5% RTP fibre.

**Table 3** Mix proportions of specimens used in this study.

Mix ID	Weight ratio				Volume (%)		
	Binder		Sand/ binder	Activator/ binder	SP/binder	PVA fibre	RTP fibre
	Fly ash	Slag					
0P-0R						0	0
1.0P-0R						1.0	0
1.5P-0R	0.8	0.2	0.2	0.45	0.01	1.5	0
2.0P-0R						2.0	0
1.75P-0.25R						1.75	0.25

1.5P-0.5R	1.5	0.5
1.25P-0.75R	1.25	0.75
1.0P-1.0R	1.0	1.0

Note: SP = superplasticiser.

### 2.3. Sample preparation

The adopted mixing process for all EGC samples is displayed in Fig. 4. For mixtures containing RTP fibres, the RTP fibres were first blended with a proportion of alkaline activator before adding into the mixer, which can help disperse the fibres uniformly (Chen et al., 2021; Onuaguluchi and Banthia, 2017; Zhong and Zhang, 2021). The entire mixing process lasted about 10 min. The prepared mixture was then cast into cylindrical moulds ( $\varnothing$  100 mm  $\times$  50 mm) and cured at ambient temperature ( $20 \pm 2$  °C) for 24 h. After demoulding, all samples were stored in a standard curing room ( $20 \pm 2$  °C, 95% RH) until 28 d.

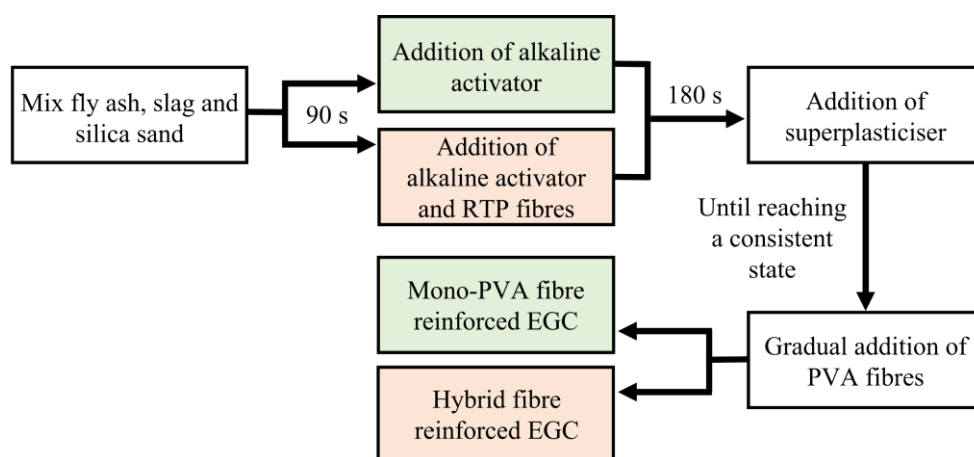


**Fig. 4.** Mixing process for mono-fibre and hybrid fibre engineered geopolymer composites (EGC).

### 2.4. Test methods

#### 2.4.1. Quasi-static splitting tensile test

The quasi-static splitting tensile test was conducted on three cylindrical specimens with dimension of  $\varnothing$  100 mm  $\times$  50 mm (Chen et al., 2020; Khan et al., 2019; Lai et al., 2022), which were different from that ( $\varnothing$  100 mm  $\times$  200 mm) specified by ASTM C496 (2017). The used dimension here was kept consistent with that for the dynamic splitting tension test to gain reliable DIF values, as indicated in previous studies (Chen et al., 2020; Khan et al., 2019). During the test, a vertical load along the diameter of the tested sample was applied at a constant loading rate of 0.5 mm/min. Besides, two pieces of plywood were placed between the loading plates and the tested specimen to avoid stress localisation at the loading point, which can help achieve a more uniform stress distribution (ASTM C496, 2017).

#### 2.4.2. Dynamic splitting tensile test

As explained in [Section 1](#), the SHPB apparatus was used in this study to explore the tensile behaviour of EGC under various strain rates, the schematic diagram and photograph of which are shown in [Fig. 5](#). The SHPB system mainly consists of a striker bar, an incident bar, a transmission bar and the data processing system. During the SHPB test, the striker impacted the incident bar under the action of compressed nitrogen with different pressure levels (0.4-0.8 MPa) to produce an incident pulse. When the incident pulse propagated to the interface between the incident bar and the tested sample, a proportion of the incident pulse was reflected as reflected pulse because of the mismatch of wave impedance ([Chen and Song, 2011](#)), and the remaining pulse continued to propagate along the transmission bar named transmission pulse. The strain gauges mounted on the incident and transmission bars were employed to collect these pulses, i.e.,  $\varepsilon_i(t)$ ,  $\varepsilon_r(t)$  and  $\varepsilon_t(t)$ . The generated impact velocities were measured using the speed detection device installed at the end of the launch tube. A pulse shaper with a diameter of 30 mm and a thickness of 3 mm was used to achieve the dynamic stress equilibrium, as shown in [Fig. 5](#) ([Zhong and Zhang, 2022b](#)). [Fig. 6](#) depicts an example of verifying the stress equilibrium of the tested sample, indicating that the sum of incident pulse and reflected pulse was close to the transmission pulse during the dynamic splitting tension, which confirms the attainment of the equilibrium stress state.

According to the one-dimension elastic stress wave theory, the dynamic splitting stress history ( $\sigma_{dt}(t)$ ) and relative displacement history of the two ends of the tested sample along the loading direction ( $u(t)$ ) can be calculated as ([Chen and Song, 2011](#); [Wu et al., 2014](#)):

$$\begin{cases} \sigma_{dt}(t) = \frac{2F_{dt}(t)}{\pi D_s L_s} \\ F_{dt}(t) = \frac{E_b A_b}{2} (\varepsilon_i(t) + \varepsilon_r(t) + \varepsilon_t(t)) \\ u(t) = C_b \int_0^t (\varepsilon_i(t) - \varepsilon_r(t) - \varepsilon_t(t)) dt \end{cases} \quad (1)$$

where  $F_{dt}(t)$  is the average dynamic splitting tensile force history acting on the tested specimen,  $E_b$ ,  $A_b$  and  $C_b$  are the elastic modulus, cross-sectional area and longitudinal wave velocity of the SHPB bar, and  $D_s$  and  $L_s$  denote the diameter and length of the tested specimen.

For each test, the strain rate ( $\dot{\varepsilon}$ ) was derived using the following equation:

$$\dot{\varepsilon} = \frac{f_{dt}}{t_0 E_s} \quad (2)$$

where  $f_{dt}$  corresponds to the dynamic splitting tensile strength,  $t_0$  represents the time needed to achieve the peak of transmission stress, and  $E_s$  is the elastic modulus of the tested specimen.

The energy absorption capacity of the tested sample during dynamic splitting tension ( $W_{dt}$ ) can be calculated by ([Chen et al., 2020](#)):

$$W_{dt} = E_b A_b C_b \int_0^t (\varepsilon_i^2(t) - \varepsilon_r^2(t) - \varepsilon_t^2(t)) dt \quad (3)$$

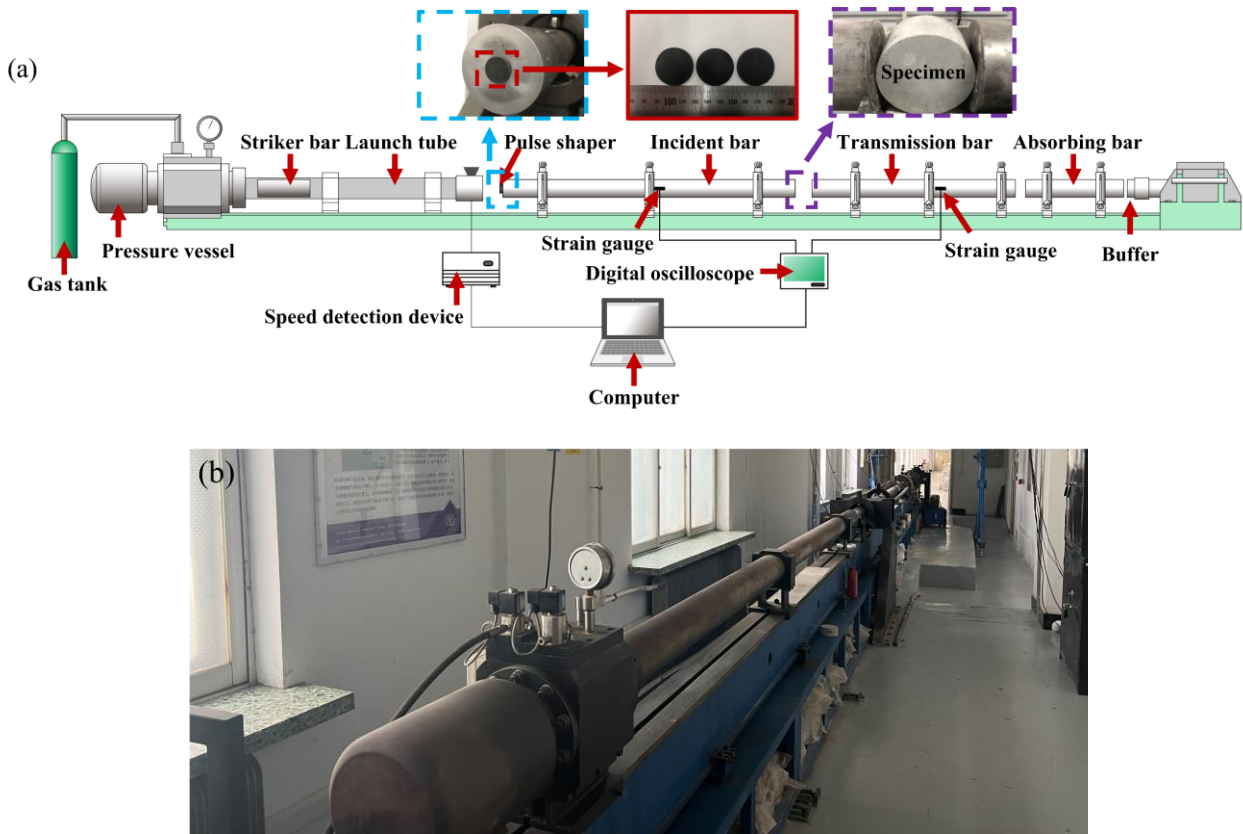


**Fig. 5.** Split Hopkinson pressure bar (SHPB) system: (a) schematic illustration, and (b) photo of the actual device.

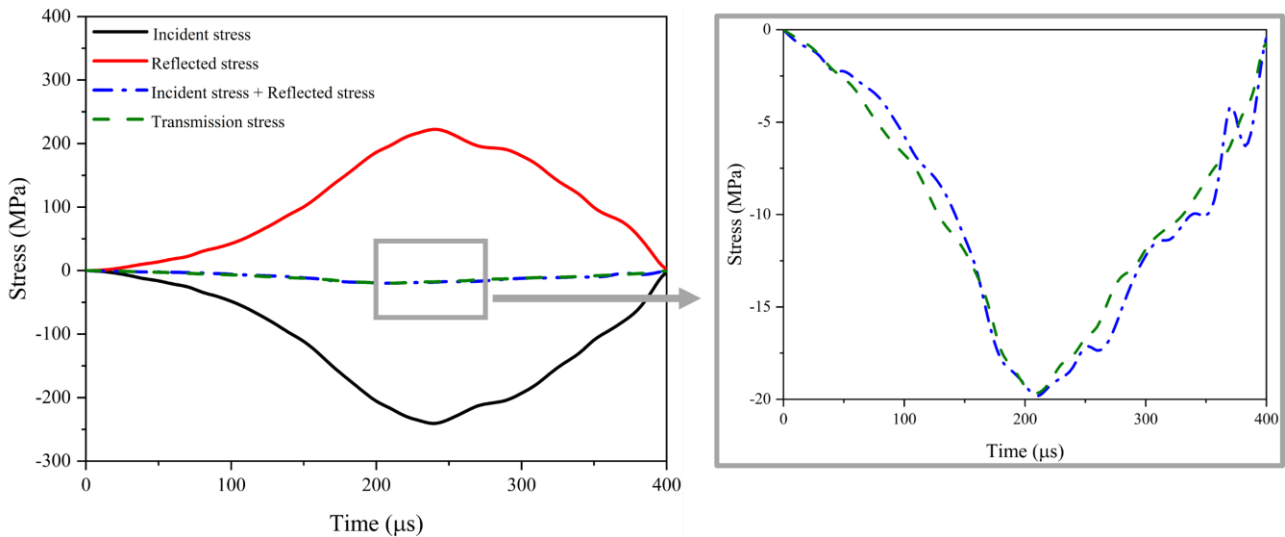


**Fig. 6.** Typical stress equilibrium verification for SHPB test.

#### 2.4.3. Microstructure characterisation

To detect the fibre failure morphology after SHPB tests, a handheld digital microscope and SEM (FEI, QUANTA FEG 250, USA) were applied. For SEM imaging, several small pieces of EGC samples after dynamic splitting tension were carefully extracted and then used for scanning. In addition, X-ray computed tomography (XCT) test was conducted to characterise the pore structure and fibre

distribution of 2.0P-0R and 1.75P-0.25R to gain insight into their relations with mechanical properties. A small block was cut from the middle section of the dog-bone shaped EGC specimen for XCT imaging with a resolution of about 6.8  $\mu\text{m}/\text{voxel}$ . The XCT data was processed using VG Studio to reconstruct 3D pore structure and evaluate pore size distribution. The global thresholding method based on the grey value of images was employed to segment different phases in EGC ([Zeng et al., 2019](#)).

### 3. Results and discussion

#### 3.1. Quasi-static splitting tensile strength

**Fig. 7** presents the quasi-static splitting tensile strength of all mixtures and the corresponding results of uniaxial tensile strength ([Zhong and Zhang, 2021](#)) were also plotted for comparison. Similar to the trend of uniaxial tensile strength, the splitting tensile strength of EGC went up with the increasing PVA fibre dosage and dropped with the increase of RTP fibre replacement level. For instance, the splitting tensile strength of 2.0P-0R was 196.09% and 29.05% higher than that of plain geopolymer mixture and EGC with 1.0% PVA fibre, while the splitting tensile strengths of 1.75P-0.25R and 1.0P-1.0R were 3.36% and 18.40% lower as opposed to 2.0P-0R. When the fibre dosage within a specimen is higher, the splitting tensile strength tends to be larger as more fibres can exert the bridging effects to limit the crack development along the loading direction until fibre pull-out or fibre rupture. RTP fibres are more effective in controlling induced micro-cracks because of their shorter length, lower strength and poorer interfacial bonding with the matrix compared to PVA fibres ([Zhong and Zhang, 2021, 2022b](#)). Hence, hybrid fibre reinforced EGC possessed a lower load-carrying capacity than mono-PVA fibre reinforced EGC. The synergistic effect of hybrid PVA and RTP fibres still can effectively control the crack development at different scales, which can explain the insignificant weakening effect in splitting tensile strength of EGC induced by the presence of a certain dosage of RTP fibre (0.25-0.5%).

**Fig. 8** illustrates the typical failure modes of plain geopolymer and EGC, indicating that the plain geopolymer was split into two halves while the EGC specimen maintained its structural integrity accompanied by a main major crack (red solid line) and some diffuse micro-cracks (red dash line). During the splitting tensile loading, the tensile stress would mainly appear along the diameter of the tested specimen (i.e., loading direction), where the tangential stress would exceed the uniaxial tensile strength and lead to failure ([Chen et al., 2014](#)). Hence, the major crack of the failed specimen would lie within the central portion. Under the action of fibre bridging, the crack development path of EGC was not straight (**Fig. 8b**), which was different from that of plain geopolymer (i.e., almost vertical). The appearance of diffuse micro-cracks near the major crack could be because the bridging fibres dispersed the tensile stress to surrounding areas of the major crack ([Chen et al., 2020](#)). Based on the image of fibre conditions at the crack interface after the quasi-static splitting tension, PVA fibres

were either pulled out or ruptured as the development of the major crack. These fibre failure conditions were similar to those after the uniaxial tension (Zhang and Zhang, 2021), where the pull-out of PVA fibre was more favourable for strength improvement. Besides, many matrix fragments adhered to the surface of the pulled out PVA fibre indicate its strong interfacial bonding with the geopolymer matrix, which can prevent the macro-crack from propagation. By contrast, the surface of the RTP fibre did not have any distinct matrix particle due to its hydrophobic surface feature, where the hydrophobic behaviour can be evidenced by its water contact angle (larger than  $130^\circ$ ) shown in Fig. 9. However, it still can restrain the initiated internal micro-crack and prevent it from coalescence into a macro-crack.

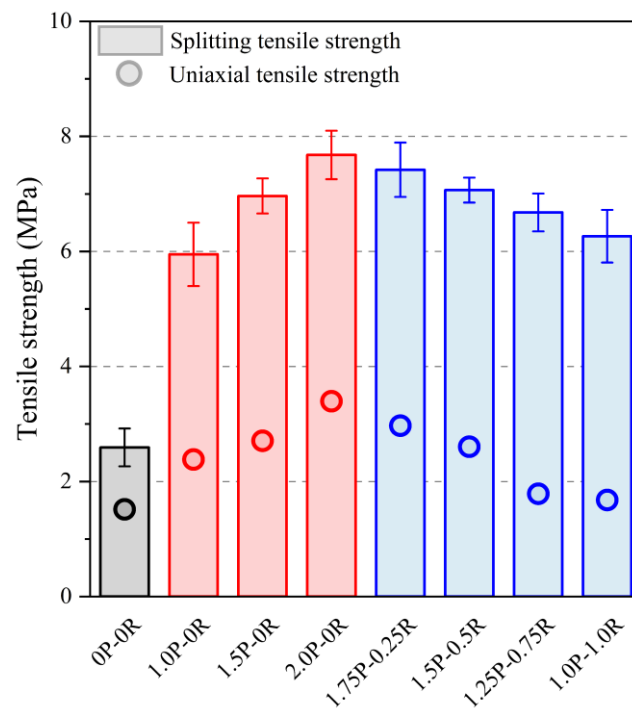


Fig. 7. Quasi-static tensile strength of all mixtures.

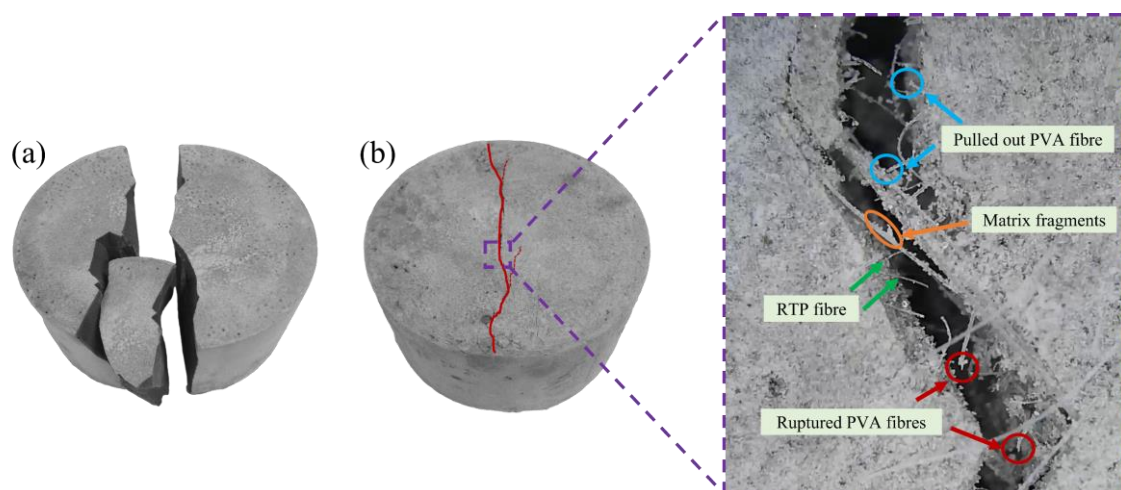
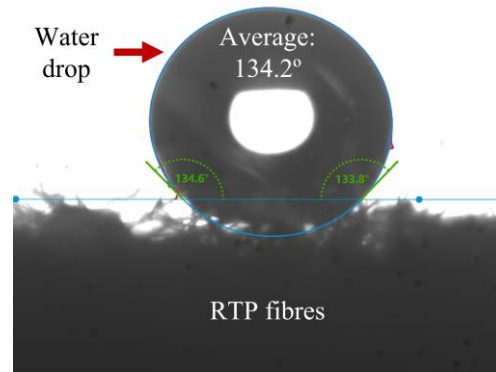


Fig. 8. Typical tensile failure patterns of (a) plain geopolymer, and (b) hybrid fibre reinforced EGC.



**Fig. 9.** Water contact angle of RTP fibres.

### 3.2. Failure pattern

#### 3.2.1. Effect of strain rate

The typical failure modes of all mixtures under various strain rates are presented in [Figs. 10](#) and [11](#). In general, similar to the failure specimens under dynamic compression ([Zhong and Zhang, 2022b](#)), the failure patterns of all mixtures here were strain-rate dependent. As mentioned early, the major crack should mostly pass through the centre of the specimen whilst the splitting tensile loading. However, as seen in [Fig. 10a](#), the plain geopolymer exhibited pronounced fragmental failure when the strain rate was within  $0.94\text{--}2.77\text{ s}^{-1}$ . More small fragments can be identified near the two ends of specimens. For instance, at the strain rate of  $0.94\text{ s}^{-1}$ , two large and almost symmetric fragments can be seen within the central portion of the specimen, implying that the first visible crack occurred at the centre of the specimen and then started propagating towards the two ends. Due to the possibly increased stress concentration at the loading interfaces and high brittleness of the plain mixture ([Chen et al., 2017](#)), more macro-cracks can be generated during the propagation of the splitting crack. Therefore, when the strain rate was higher, the plain geopolymer exhibited fragmental failure instead of one vertical splitting crack passing through the centre. Similar findings were reported in previous studies ([Li et al., 2020](#); [Zhao et al., 2020](#)).

A similar change of failure pattern with strain rate can be observed for EGC specimens. When the strain rate was lower ( $2\text{--}3.2\text{ s}^{-1}$ ), the failure patterns of all EGC mixtures were similar to those after the quasi-static splitting tension, where the major splitting cracks were still bridged by the fibres. As the strain rate increased, all specimens started to disintegrate into two halves along with some spalling pieces, debris or diffuse cracks. This can be ascribed to the increased crack velocity, which can increase the crack formation and propagation rates and thus induce more micro-cracks and reduce the fibre bridging efficiency. In addition, some EGC mixtures exhibited triangular damage near the two ends of specimens at a strain rate over  $4\text{ s}^{-1}$ , as seen in [Fig. 10c](#). Similar phenomena were found in previous studies ([Chen et al., 2020](#); [Khan et al., 2019](#); [Li et al., 2020](#)), which can be attributed to the

limited crack initiation and development along the loading diameter as a result of the increased stress concentration near two ends.

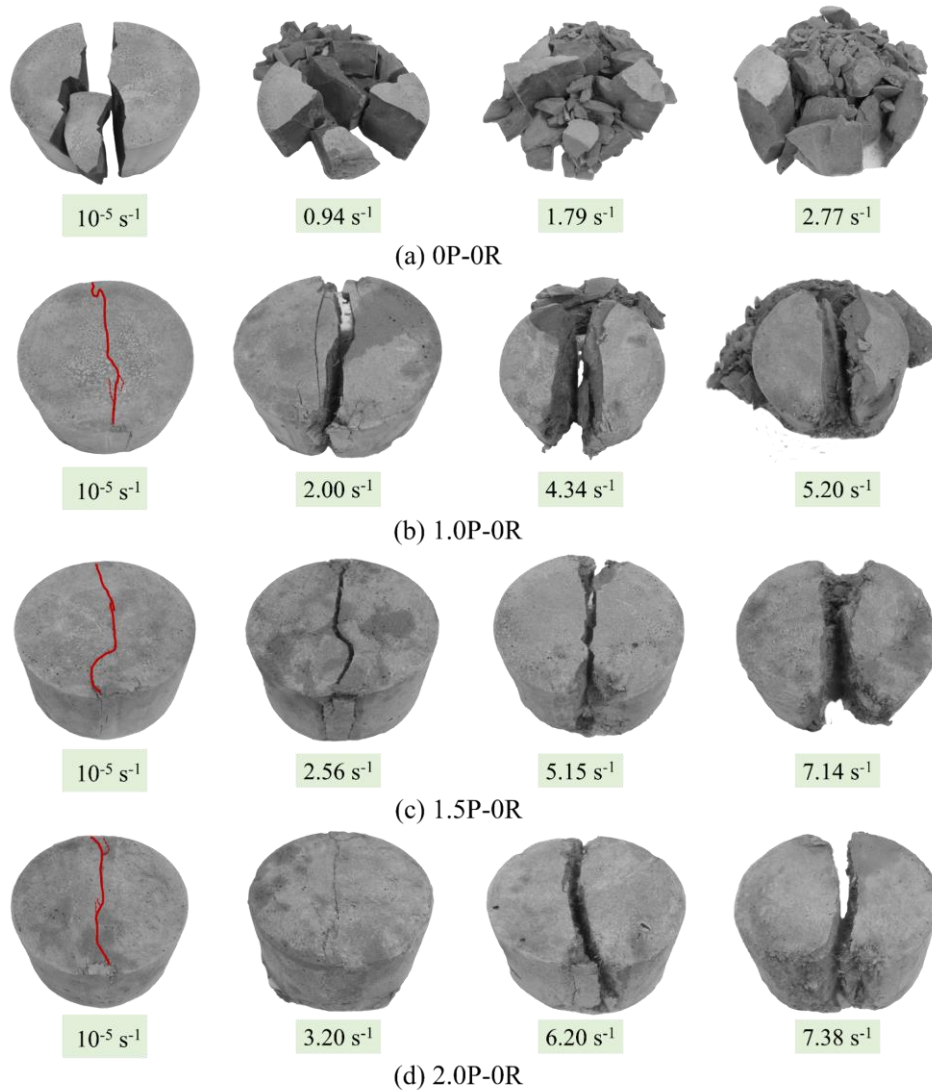


**Fig. 10.** Typical failure modes of plain geopolymer and mono-PVA fibre reinforced EGC under quasi-static and dynamic splitting tension.

### 3.2.2. Effect of fibre

As displayed in [Figs. 10](#) and [11](#), irrespective of fibre type and content, the inclusion of fibres significantly reduced the damage degree of samples at different strain rates as all EGC samples did not show the fragmental failure observed in plain geopolymer. When the PVA fibre dosage within the specimen was higher, the damage level caused by the dynamic splitting tension was lower. At a strain rate of 2-3.2  $s^{-1}$ , 1.0P-0R fractured into almost two halves along with a very tiny number of fibres bridging the major splitting crack ([Fig. 10b](#)), while the crack width of the splitting crack for 1.5P-0R was much smaller and more bridging PVA fibres appeared at the crack interface ([Fig. 10c](#)). The integrity loss of 2.0P-0R was the lowest as compared with 1.0P-0R and 1.5P-0R, which can be ascribed to the higher number of effective bridging fibres at the crack interface ([Khan et al., 2019](#); [Lai et al., 2022](#)). As mentioned in [Section 3.2.1](#), all mono-PVA fibre reinforced EGC mixtures were

broken into two halves at a higher strain rate but the increase of PVA fibre dosage still can mitigate the damage. For instance, the failed sample of 1.0P-0R had many spalling pieces and debris, while 1.5P-0R and 2.0P-0R did not show such phenomenon under a similar strain rate. However, altering the PVA fibre dosage did not have an apparent effect on reducing the triangular damage degree of specimens, especially within a strain rate of  $5.2\text{-}7.38\text{ s}^{-1}$ . A similar finding was reported in previous studies that increasing either steel fibre content ([Hao and Hao, 2016](#); [Khan et al., 2019](#)) or RTP fibre dosage ([Chen et al., 2020](#)) in cementitious or geopolymer materials did not considerably mitigate the triangular damage near the loading ends.

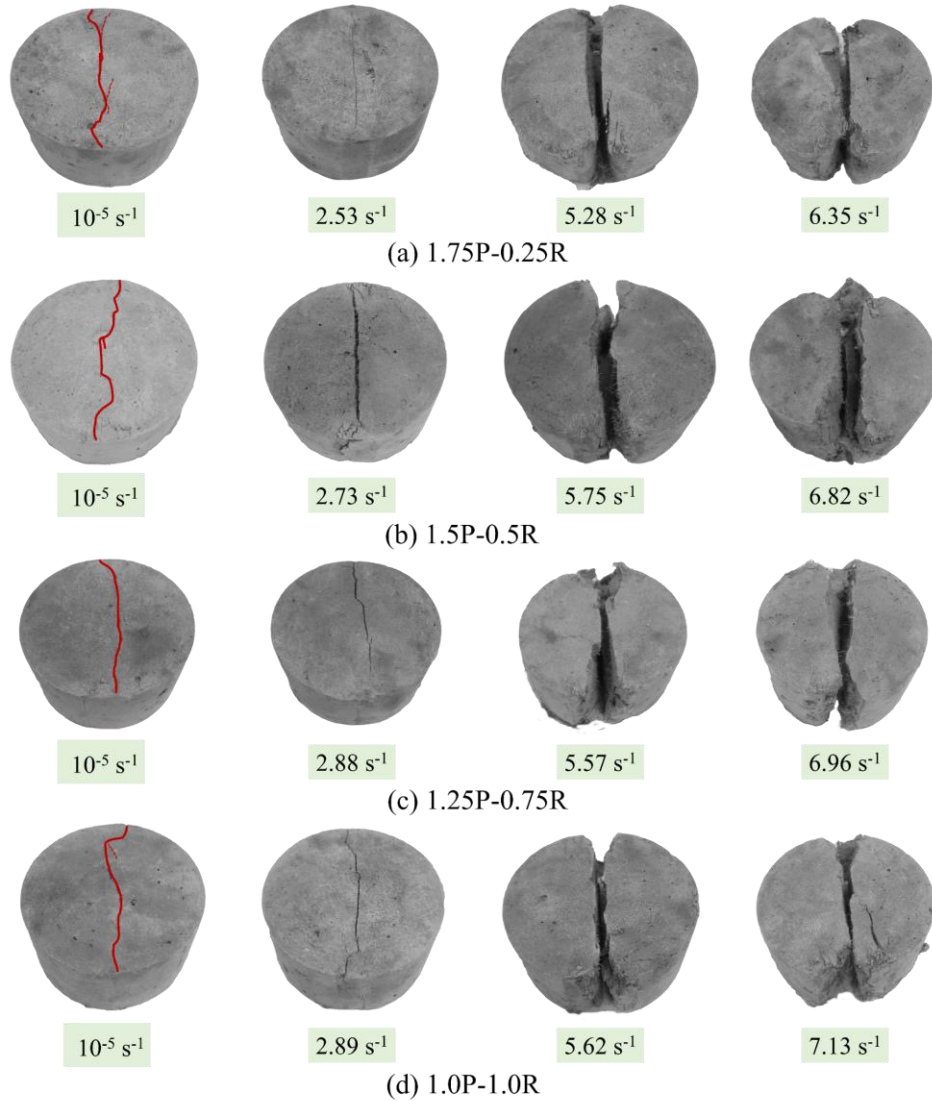


**Fig. 11.** Typical failure modes of hybrid fibre reinforced EGC under quasi-static and dynamic splitting tension.

**Fig. 11** indicates that the failure patterns of all hybrid fibre reinforced EGC were comparable with that of EGC incorporating 2.0% PVA fibre at different strain rates as no significant spalling pieces and debris were identified. This can be ascribed to the synergistic effect of hybrid fibres in limiting cracks, as discussed in [Section 3.1](#). Less diffuse cracks can be distinguished on the failed EGC

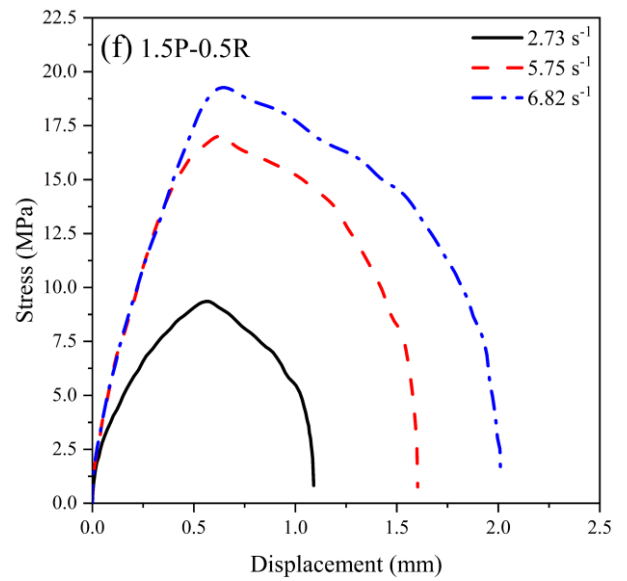
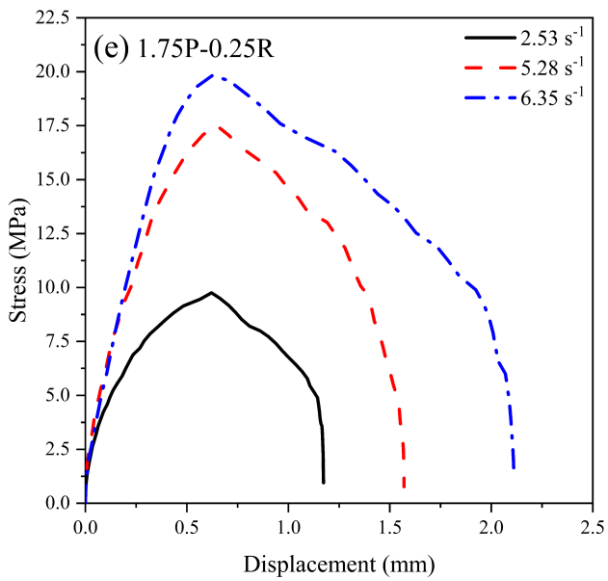
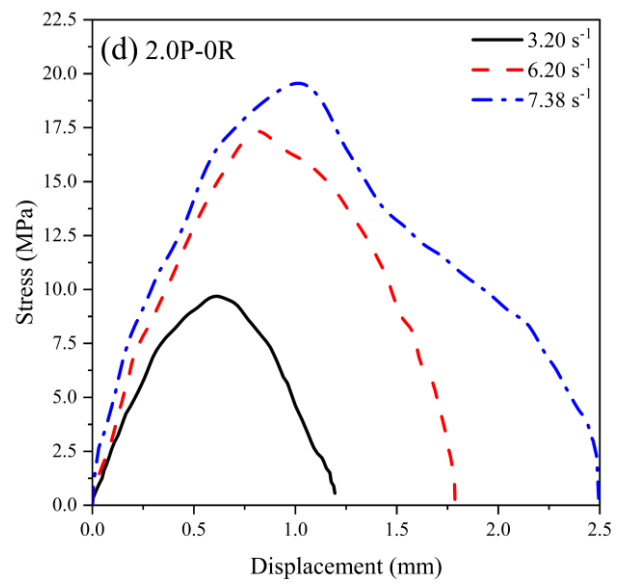
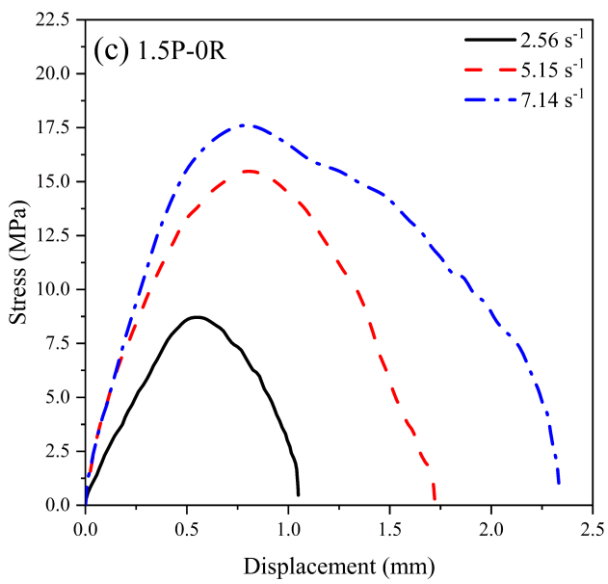
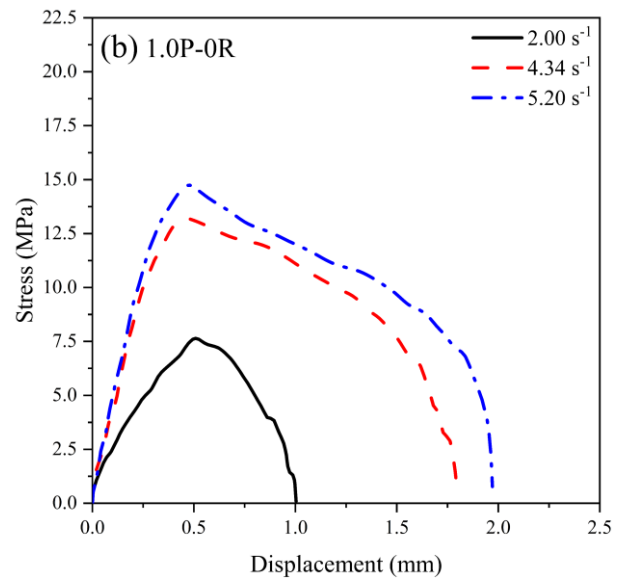
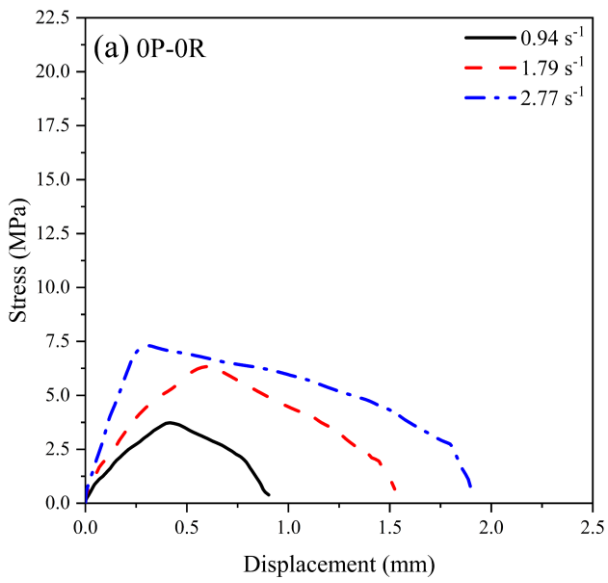
specimens at a higher strain rate because of the larger fracture propagation rate. Thus, most fibres did not have enough time to disperse the splitting tensile stress as they were either pulled out or ruptured quickly as the growth of the major splitting crack ([Zhong and Zhang, 2022b](#)). Overall, the presented failure modes here can reveal the positive influence of fibres in enhancing the dynamic splitting tensile behaviour as compared with plain geopolymer, while it should be further verified with qualitative analyses below.

### 3.3. Dynamic splitting tensile strength

#### 3.3.1. Effect of strain rate

**Fig. 12** displays the typical dynamic splitting tensile stress against relative displacement calculated using **Eq. (1)** for all mixtures at different strain rates. All curves had a similar shape consisting of ascending and descending stages. Within the ascending region, the dynamic splitting tensile stress would first increase linearly with the increase of relative displacement before moving into the non-linear stress increment stage. The first visible crack usually appears during this non-linear region ([Lai et al., 2022](#)). Then, the crack would propagate towards two ends of the specimen, and the fibres start exerting their crack-controlling functions for EGC mixtures.

The dynamic splitting tensile strength (i.e., peak dynamic splitting tensile stress) of all mixtures was sensitive to the strain rate. For instance, the dynamic splitting tensile strength of 2.0P-0R was enhanced by 78.17% and 99.97% when the strain rate increased from  $3.2 \text{ s}^{-1}$  to  $6.2 \text{ s}^{-1}$  and  $7.38 \text{ s}^{-1}$ , respectively. This can be mainly attributed to the increased crack velocity, Stefan effect and lateral inertia ([Chen et al., 2014](#); [Khan et al., 2019](#)). As mentioned in **Section 3.2.1**, the enhanced crack velocity induced by the increase of strain rate would lead to higher crack initiation and proliferation rates, which can be evidenced by **Fig. 12** that the slope of the curve was larger at a higher strain rate. More micro-cracks are generated to consume the energy, improving the strength. For the Stefan effect, the reaction force caused by the free water trapped between the crack is proportional to the crack velocity ([Chen et al., 2014](#)), which would contribute to the strength improvement as the increase of strain rate. Although it was reported that using the specimen with an aspect ratio of 0.5 for the SHPB test can eliminate the inertia effect ([Bertholf and Karnes, 1975](#); [Khan et al., 2018](#)), these findings were mainly valid for the dynamic compression test. Therefore, the observed strength enhancement here could be partly caused by the lateral inertia effect.



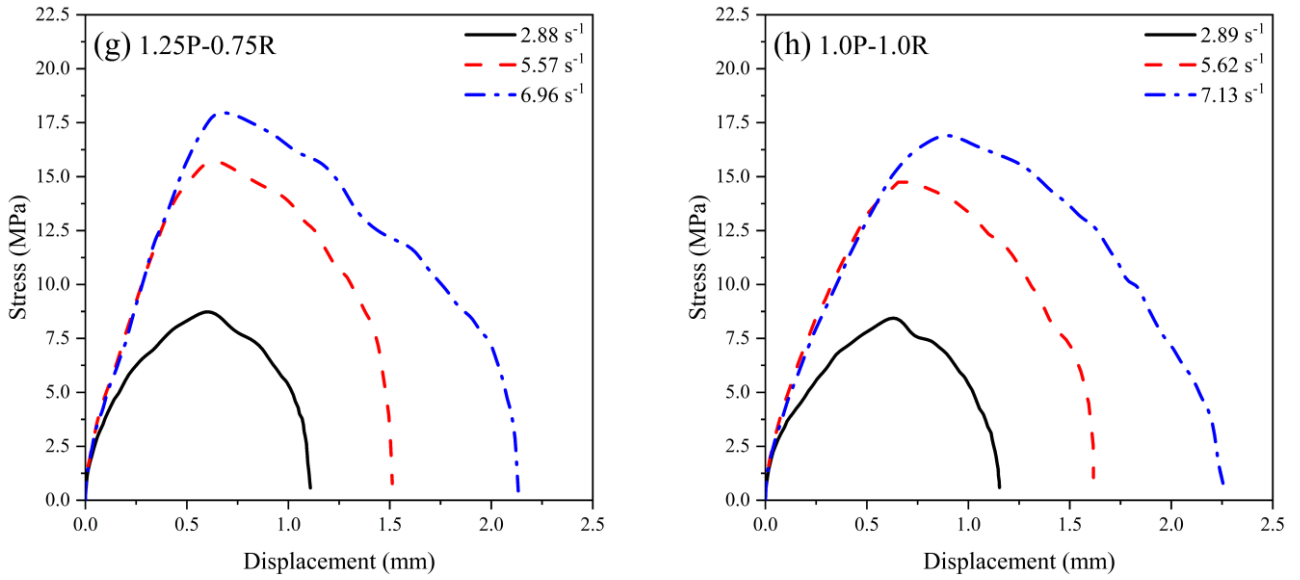


**Fig. 12.** Dynamic splitting tensile stress against relative displacement for all mixtures.

### 3.3.2. Effect of fibre

The effects of PVA and RTP fibres on the dynamic splitting tensile strength of EGC at different strain rates are shown in Fig. 13. Similar to quasi-static splitting tensile strength, the presence of fibres significantly enhanced the dynamic splitting tensile strength of geopolymers at various strain rates. For instance, the dynamic splitting tensile strengths of 2.0P-0R and 1.0P-1.0R were 154.88% and 120.36% higher than that of 0P-0R within a strain rate of 0.94-3.2 s<sup>-1</sup>. The dynamic splitting tensile strength of EGC tended to be larger when the PVA fibre dosage was higher. At a strain rate of 4.34-6.2 s<sup>-1</sup>, the dynamic splitting tensile strength of 2.0P-0R was 11.95% and 31.31% higher than that of 1.5P-0R and 1.0P-0R, which can be ascribed to the enhanced fibre bridging behaviour at the crack interface. Under dynamic loading, the mechanical properties of PVA fibres and the bonding between fibres and matrix were enhanced with the rising strain rate (Curosu et al., 2016; Yang and Li, 2014), which would improve the fibre bridging efficiency and resulted in more pulled out PVA fibres. Thus, a more obvious strength enhancement of mono-PVA fibre reinforced EGC over plain geopolymer under dynamic loading can be found than that under quasi-static loading. Nevertheless, inconsistent results were observed in this study. For instance, the quasi-static splitting tensile strength of 1.5P-0R was about 169% higher than that of 0P-0R, while the corresponding dynamic splitting tensile strength was only 129.42-144.33% greater. This is because the crushing damage on plain geopolymer was more significant in comparison with EGC mixtures (see Fig. 10a), which would overestimate its dynamic splitting tensile strength. Furthermore, the strength enhancement of mono-PVA fibre reinforced EGC over plain geopolymer declined slightly when the used nitrogen pressure level changed from 0.6 MPa to 0.8 MPa, which can be associated with the increased number of ruptured PVA fibres caused by the superior interface properties of PVA fibres at a higher strain rate and

thereby weakening the fibre bridging efficiency ([Zhong and Zhang, 2022b](#)). In addition, fibres tend to rupture when their inclination angles are too large ([Li, 2019](#)).

On the other hand, replacing PVA fibre with a small dosage of RTP fibre (0.25-0.5%) resulted in comparable or slightly better dynamic splitting tensile strength compared to 2.0P-0R (no more than 3.42% difference between them). Under quasi-static loading, the splitting tensile strength of 1.75P-0.25R was 3.36% lower than that of 2.0P-0R, while 1.75P-0.25R outperformed 2.0P-0R in terms of dynamic splitting tensile strength when the strain rate was within  $1.79\text{-}7.38\text{ s}^{-1}$ . This can be mainly ascribed to the improved synergistic effect of hybrid fibres in restraining the cracks under dynamic loading caused by the increased fibre properties and better fibre distribution ([Zhong and Zhang, 2022b](#)). The smaller spacing between RTP fibres can contribute to the improved efficiency of such synergistic effect ([Chen et al., 2021](#); [Zhong and Zhang, 2022b](#)). Because of the hydrophobic feature of RTP fibres, more free water may be retained within the matrix of EGC. As such, the Stefan effect can be intensified to improve strength. Nevertheless, when the RTP fibre replacement level was higher than 0.5%, the dynamic splitting tensile strengths of 1.25P-0.75R and 1.0P-1.0R were 7.87-10.36% and 13.41-14.55% lower than that of 2.0P-0R under different strain rates. This is because RTP fibres are more efficient in controlling the micro-cracks (see [Section 3.1](#)). When these micro-cracks grow into macro-cracks, fewer PVA fibres can arrest and bridge them as the total number of PVA fibres is lower at a higher RTP fibre replacement level. Besides, the fibre distribution of these EGC mixtures could be poorer as a result of lower workability, which can weaken the synergistic effect of hybrid fibres and thus strength ([Zhong and Zhang, 2021](#)).

[Fig. 14](#) shows the fibre conditions at the crack interface under dynamic splitting tension. Similar to the fibre conditions under quasi-static loading, both pulled out and ruptured PVA fibres can be captured when the strain rate was lower, and most fibres still bridged the crack ([Fig. 14a](#)). By contrast, when the strain rate was higher, almost no fibres bridged the crack due to the increasing crack width. Many pulled out PVA fibres with a long pull-out length can be identified. Although the ruptured PVA fibre still can be found, it can be assumed that its total proportion was smaller than that at a lower strain rate, which is consistent with the finding reported in a previous study ([Trindade et al., 2020](#)) that most PVA fibres in EGC were pulled out under dynamic tension. As seen in [Fig. 14b](#), there was no pronounced change in terms of the RTP fibre failure condition with the change of strain rate, implying that RTP fibres still presented a pull-out feature though their properties were also enhanced with strain rate. Less bridging RTP fibres can be observed near the crack interface at a lower strain rate, which confirms the previous discussion that RTP fibres are not effective in restraining the macro-cracks. To this end, the dosage of RTP fibre in EGC should be limited to ensure the acceptable crack-controlling ability for hybrid fibre reinforced EGC under dynamic loading.

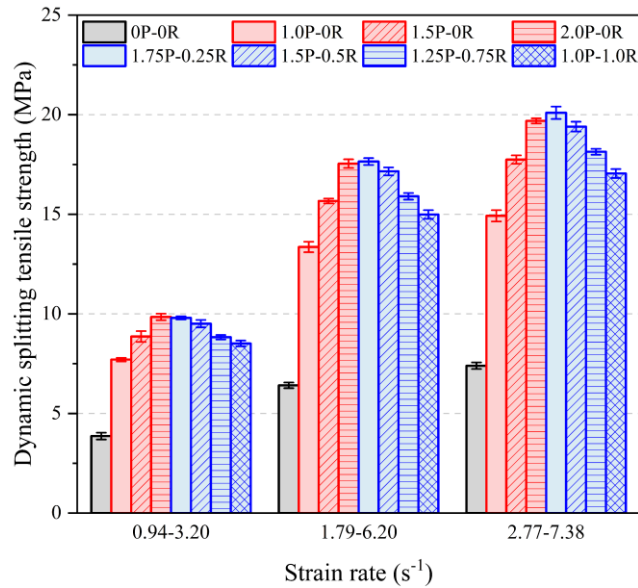


**Fig. 13.** Dynamic splitting tensile strength of all mixtures.

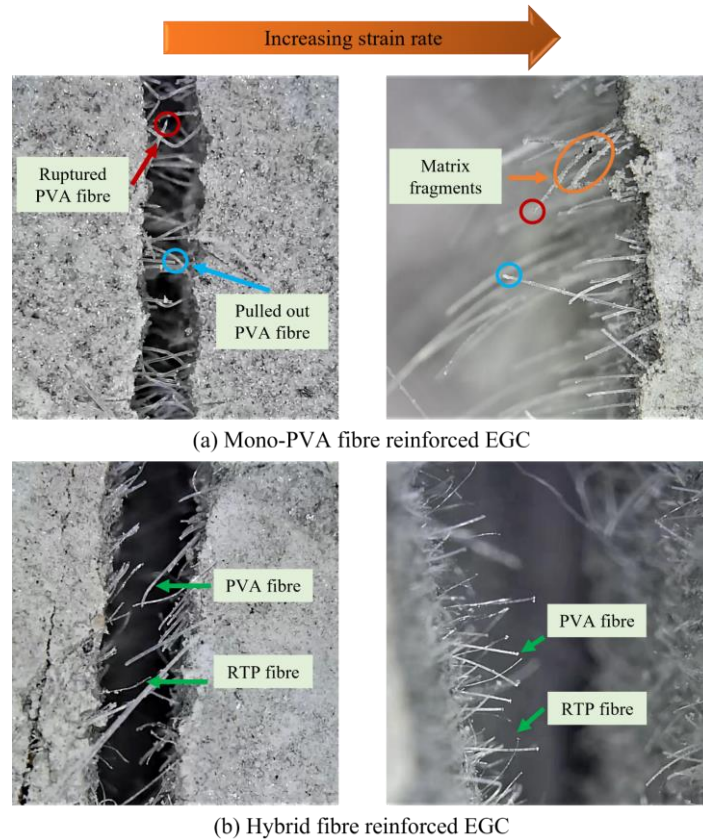


**Fig. 14.** Fibre conditions under dynamic splitting tension.

### 3.4. Dynamic increase factor

#### 3.4.1. Effect of strain rate

DIF is usually used to quantify the strength enhancement under dynamic loading and it is essential to describe the relationship between DIF and strain rate, which can guide the optimal structural design and offer insight for numerical analysis (Chen et al., 2020; Wu et al., 2017). Fig. 15 illustrates the proposed DIF equations for all studied mixtures, indicating that a transition rate existed for all mixtures. After that, DIF went up considerably with the increasing strain rate, which is consistent

with the changing trend of dynamic splitting tensile strength with strain rate. It is worth mentioning that the transition rates for all EGC mixtures ( $2.09\text{-}3.28\text{ s}^{-1}$ ) were higher than that for plain geopolymer ( $1.03\text{ s}^{-1}$ ), which can be ascribed to the larger activating rate required for fibre reinforced composites to alter their properties as a result of fibre bridging behaviour ([Wang et al., 2011](#)). The resulted strain rate for plain geopolymer was lower than that for EGC under the same nitrogen pressure level. A similar finding was presented in a previous study ([Lai et al., 2022](#)) that the obtained strain rate for plain concrete was slightly lower than that for the mixtures containing steel fibres or rubber particles mainly due to the changes of elastic modulus and density. Given the equation for calculating the strain rate, i.e., [Eq. \(2\)](#), it can be found that the determined strain rate can be strongly affected by elastic modulus. Overall, the developed DIF equations here had high reliability with  $R^2$  of mostly greater than 0.9.

#### 3.4.2. Effect of fibre

Plain geopolymer was more sensitive to strain rate as indicated in the largest gradient of the proposed first-part equation (see [Fig. 15a](#)). The serious crushing damage on plain geopolymer can overestimate its dynamic splitting tensile strength, leading to a higher strength enhancement rate. Additionally, as seen in [Figs. 10](#) and [11](#), most EGC mixtures maintained the structural integrity with many bridging fibres at the crack interfaces when the strain rate was within  $2\text{-}3.2\text{ s}^{-1}$ , which can considerably restrain the formation of micro-cracks, weakening the strain rate sensitivity. Similar results were found in previous studies ([Khan et al., 2019](#); [Lai et al., 2022](#)). The moisture content plays an essential role in the region between the quasi-static strain rate and transition strain rate ([Wu et al., 2012](#)), which can explain why hybrid fibre reinforced EGC had higher strain rate sensitivity (with a gradient of over 0.07) than mono-PVA fibre reinforced EGC (with a gradient of 0.061-0.067) in this region (see [Figs. 15b-h](#)). When the strain rate exceeded the transition strain rate, 2.0P-0R and other hybrid fibre reinforced EGC mixtures possessed a more significant strain rate dependence than plain geopolymer and other mono-PVA fibre reinforced EGC mixtures, implying that the fibre bridging and pull-out behaviour play an important role in enhancing the strain rate sensitivity during this region. It was also found in a previous study ([Hao and Hao, 2016](#)) that the pull-out behaviour of spiral steel fibres significantly improved the strain rate sensitivity of normal concrete.

#### 3.4.3. Comparison with existing DIF models

[Fig. 16](#) demonstrates a comparison of the obtained DIF results in this study with the predictions by the existing DIF models for cementitious materials. The DIF model given in [CEB-FIP model code 1990: Design code \(1990\)](#) has been widely used to describe the strain rate effect on the strength rise of normal concrete up to  $300\text{ s}^{-1}$ :

$$\begin{cases} DIF_{CEB-FIP} = \left(\frac{\dot{\epsilon}}{\dot{\epsilon}_1}\right)^{1.016\alpha} \text{ for } \dot{\epsilon} \leq 30 \text{ s}^{-1} \\ DIF_{CEB-FIP} = \gamma \left(\frac{\dot{\epsilon}}{\dot{\epsilon}_1}\right)^{\frac{1}{3}} \text{ for } \dot{\epsilon} > 30 \text{ s}^{-1} \end{cases} \quad (4)$$

where  $\dot{\epsilon}_1$  is equal to  $0.000003 \text{ s}^{-1}$ ,  $\alpha$  is  $(10 + 6 \frac{f_c}{f_{c1}})^{-1}$ ,  $\gamma$  is  $10^{(7.11\alpha - 2.33)}$ ,  $f_c$  denotes the quasi-static compressive strength, and  $f_{c1} = 10 \text{ MPa}$ .

It can be seen that the CEB-FIP model takes the quasi-static compressive strength into account, and 50 MPa was used as the input. Later on, [Malvar and Ross \(1998\)](#) found that the CEB-FIP model was not reliable for estimating the strain rate sensitivity of normal concrete at high strain rates and thus proposed a new model with a lower transition rate, as follows:

$$\begin{cases} DIF_{M\&R} = \left(\frac{\dot{\epsilon}}{\dot{\epsilon}_1}\right)^\alpha \text{ for } \dot{\epsilon} \leq 1 \text{ s}^{-1} \\ DIF_{M\&R} = \gamma \left(\frac{\dot{\epsilon}}{\dot{\epsilon}_1}\right)^{\frac{1}{3}} \text{ for } \dot{\epsilon} > 1 \text{ s}^{-1} \end{cases} \quad (5)$$

where  $\dot{\epsilon}_1$  is equal to  $0.000001 \text{ s}^{-1}$ ,  $\alpha$  is  $(1 + 8 \frac{f_c}{f_{c1}})^{-1}$ , and  $\gamma$  is  $10^{(6\alpha - 2)}$ .

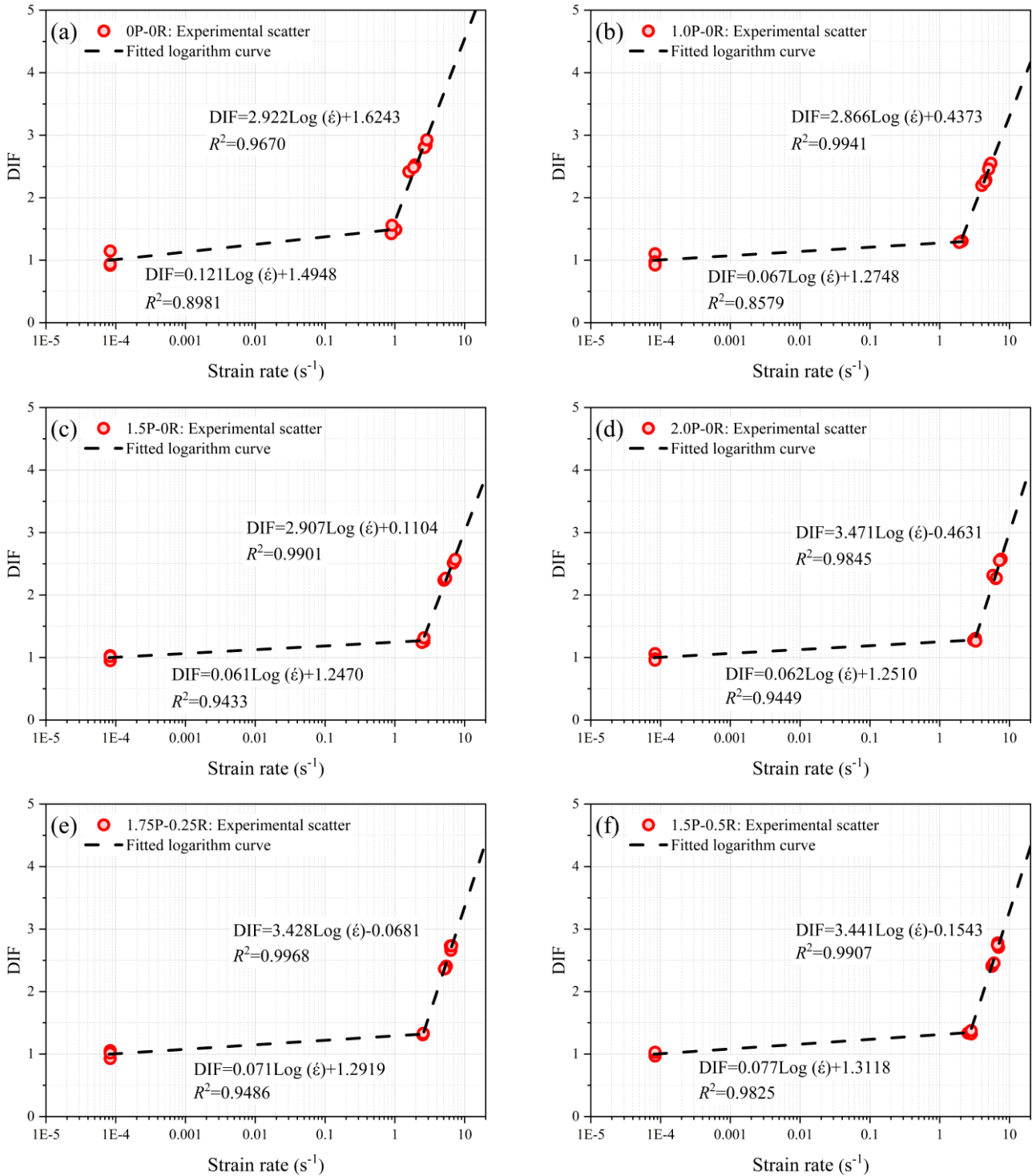
The [FIB Model Code for Concrete Structures 2010 \(2013\)](#) was also used for comparison:

$$\begin{cases} DIF_{FIB} = \left(\frac{\dot{\epsilon}}{\dot{\epsilon}_1}\right)^{0.018} \text{ for } \dot{\epsilon} \leq 10 \text{ s}^{-1} \\ DIF_{FIB} = 0.0062 \left(\frac{\dot{\epsilon}}{\dot{\epsilon}_1}\right)^{\frac{1}{3}} \text{ for } \dot{\epsilon} > 10 \text{ s}^{-1} \end{cases} \quad (6)$$

where  $\dot{\epsilon}_1$  is equal to  $0.000001 \text{ s}^{-1}$ .

The DIF results of EGC mixtures at the strain rate of  $2-3.2 \text{ s}^{-1}$  were close to the FIB model, while the results at higher strain rates fitted the Malvar-Ross model well. By contrast, the DIF result of plain geopolymer at the strain rate of  $0.94 \text{ s}^{-1}$  showed a good agreement with the Malvar-Ross model, while the results tended to deviate from all models presented in [Fig. 16](#) when the strain rate increased. The discrepancy between the measured DIF results and predictions by CEB-FIP and FIB models at a strain rate of over  $4 \text{ s}^{-1}$  can be ascribed to the unreliability of CEB-FIP model under high strain rates ([Malvar and Ross, 1998](#)) and the ignorance of quasi-static compressive strength in FIB model. The above three models were developed mainly based on the data of normal concrete. The microstructure and macroscopic behaviour of investigated mixes in this study were different from those of normal concrete (e.g., shrinkage and porosity), leading to some inconsistencies between model predictions and the obtained DIF results here, especially for plain geopolymer mortar. For instance, the shrinkage of plain geopolymer mortar would be greater than that of normal concrete due to the absence of coarse aggregate, which may cause more cracks generated under dynamic loading and thereby higher DIF values as opposed to normal concrete, especially at a higher strain rate. The DIF results of EGC under both ambient temperature curing and heat curing obtained from [Farooq et al. \(2022\)](#) did not fit all the

models shown in Fig. 16. The heat-cured EGC had higher DIF values (1.86-2.2) than the ambient-cured EGC (1.57-1.86) when the strain rate was around  $0.51 \text{ s}^{-1}$ , due to the higher brittleness induced by cracking as a result of shrinkage. The DIF values of ambient-cured EGC obtained by [Farooq et al. \(2022\)](#) were greater than the measured data in this study under a similar strain rate, which can be attributed to the different testing methods adopted to measure the dynamic tensile strength as well as disparate macroscopic properties, e.g., quasi-static compressive and tensile strengths.



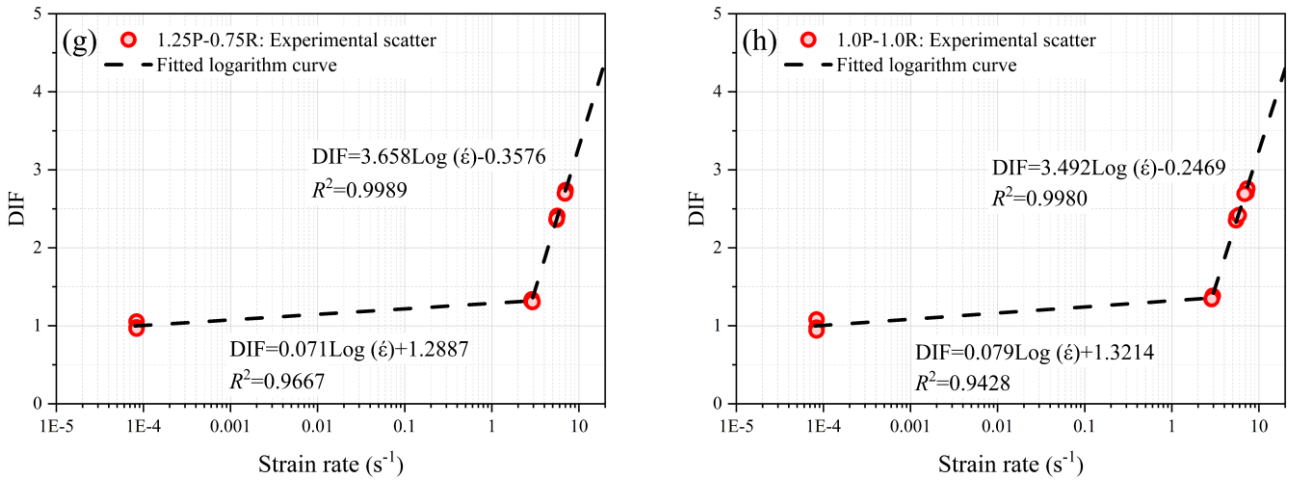


**Fig. 15.** Dynamic increase factor (DIF) as a function of strain rate: (a) 0P-0R, (b) 1.0P-0R, (c) 1.5P-0R, (d) 2.0P-0R, (e) 1.75P-0.25R, (f) 1.5P-0.5R, (g) 1.25P-0.75R, (h) 1.0P-1.0R.

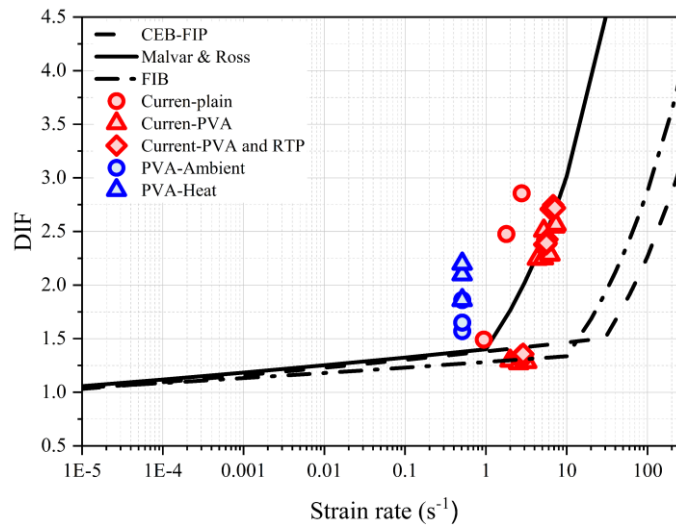


**Fig. 16.** Comparison of DIF obtained from EGC in this study with that predicted using currently existing models ([CEB-FIP model code 1990: Design code, 1990](#); [FIB Model Code for Concrete Structures 2010, 2013](#); [Malvar and Ross, 1998](#)) and that acquired from the existing study ([Faroq et al., 2022](#)).

### 3.5. Energy absorption capacity

#### 3.5.1. Effect of strain rate

**Fig. 17** presents the energy absorption capacity of all mixtures, which was determined as per the law of conservation of energy. The changing trend of energy absorption capacity was consistent with that of dynamic splitting tensile strength and DIF with strain rate. For instance, the energy absorption capacity of 0P-0R was improved by 201.25% and 357.21% when the strain rate altered from  $0.94 \text{ s}^{-1}$  to  $1.79 \text{ s}^{-1}$  and  $2.77 \text{ s}^{-1}$ , respectively. Such energy enhancement with the increasing strain rate was strongly associated with the dynamic splitting tensile strength and can be mainly attributed to the growing appearance of micro-cracks and rapid proliferation of main splitting cracks ([Chen et al., 2020](#); [Lai et al., 2022](#); [Zhao et al., 2020](#)).

### 3.5.2. Effect of fibre

Unlike plain geopolymer, an extra part of energy was required for EGC to pull out or rupture the fibres during the SHPB test. As seen in [Fig. 17](#), the presence of fibres significantly enhanced the energy absorption capacity of geopolymers under different strain rates. When the strain rate was within  $1.79\text{-}6.2\text{ s}^{-1}$ , the energy absorption capacity of 1.0P-0R, 1.5P-0R, 2.0P-0R, 1.75P-0.25R, 1.5P-0.5R, 1.25P-0.75R and 1.0P-1.0R was 159.32%, 166.33%, 201.25%, 199.38%, 204.82%, 163.71% and 158.57% higher than that of 0P-0R. The increase of PVA fibre dosage led to a higher energy absorption capacity for EGC due to the increased number of fibres experiencing the pull-out process ([Kanda and Li, 1998](#)), which shows a good agreement with the dynamic splitting tensile strength (see [Fig. 13](#)). Regarding the effect of RTP fibres, EGC mixtures containing RTP fibres outperformed EGC reinforced with 2.0% PVA fibre in terms of the energy absorption capacity when the strain rate was within  $2\text{-}3.2\text{ s}^{-1}$ . For instance, the energy absorption capacity of 1.75P-0.25R and 1.5P-0.5R was 16.83% and 1.87% higher than that of 2.0P-0R. As discussed in [Section 3.3.2](#), ruptured PVA fibres can be found at a lower strain rate, weakening the energy absorption capacity as pulled out PVA fibres are more favourable for absorbing energy. Regardless of strain rate, RTP fibres still exhibited the pull-out behaviour, which can compensate for the energy loss caused by the ruptured PVA fibres. Nevertheless, such compensation tended to be insignificant as the strain rate increased. It is worth noting that 1.75P-0.25R still can exhibit comparable energy absorption with 2.0P-0R, which is consistent with a previous study ([Lu et al., 2018b](#)) that replacing PVA fibres with hydrophobic PET fibres can lead to similar energy absorption capacity for ECC compared to ECC with 2.0% PVA fibre.

[Fig. 18](#) illustrates some SEM micrographs of PVA and RTP fibre conditions after the dynamic splitting tension test, which can offer more insights into the effect of fibre on the energy absorption capacity. It should be noted that these SEM images were taken on the samples after being subjected to the impact force with a nitrogen pressure level of 0.8 MPa. More pulled out PVA fibres can be found along with several pull-out traces and abrasion traces on the surfaces of fibres, which coincide with those shown in [Fig. 14a](#) that the fibres can considerably improve the energy absorption capacity of EGC. Owing to the strong interface properties, some ruptured PVA fibres still can be captured, which can impair the energy absorption capacity of EGC. RTP fibre still exhibited pull-out behaviour due to its weak bond with the matrix, which can be evidenced by its smooth surface. This fibre pull-out behaviour can recompense for the loss of energy absorption as a result of the ruptured PVA fibres at a lower strain rate, while such positive effect may vanish when the crack width and size become more prominent.

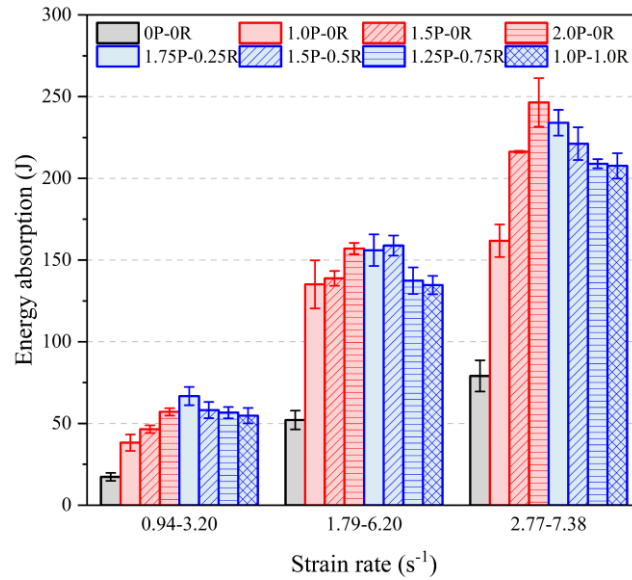


**Fig. 17.** Energy absorption capacity of all mixtures.

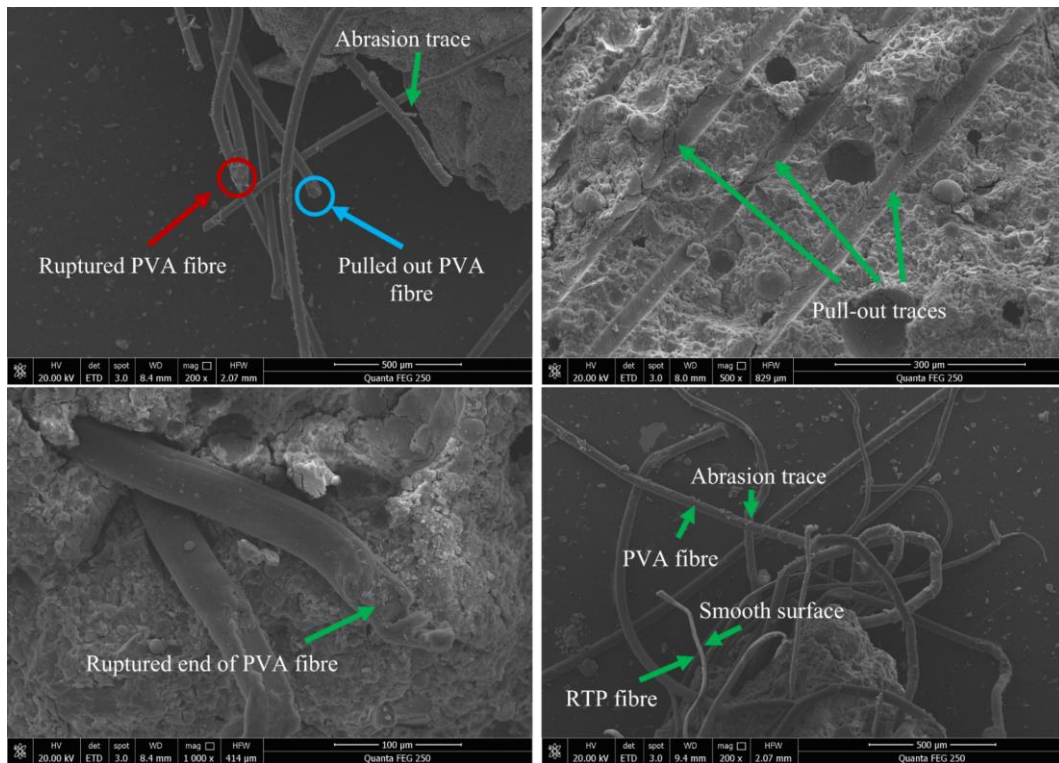


**Fig. 18.** SEM micrographs of fibre conditions under dynamic splitting tension.

#### 4. Comparisons between mono-PVA and hybrid PVA-RTP fibre reinforced EGC

An overall comparison between mono-PVA fibre reinforced EGC and hybrid PVA-RTP fibre reinforced EGC in terms of dynamic mechanical properties as well as economic and environmental benefits is presented in Fig. 19, where some results were extracted from our previous studies (Zhong and Zhang, 2021, 2022b). Uniaxial tensile properties are the essential properties of EGC and thus the uniaxial tensile strength ( $f_t$ ) and tensile strain capacity ( $\epsilon_t$ ) are also presented to better define the optimal content of RTP fibre for EGC. Overall, the presence of RTP fibres is beneficial to the dynamic mechanical properties including dynamic compressive strength ( $f_{dc}$ ) and energy absorption capacity

under both dynamic compression ( $W_{dc}$ ) and dynamic splitting tension ( $W_{dt}$ ). The elastic modulus ( $E_c$ ) of most hybrid fibre reinforced EGC is 4.87-25.56% higher than that of EGC with 2.0% PVA fibre. Replacing PVA fibres with RTP fibres is a practical approach to reduce the material cost and embodied energy of EGC, which helps promote sustainable development. Nevertheless, the uniaxial tensile properties are significantly weakened with the addition of RTP fibres. The RTP fibre dosage should be limited to 0.5% for EGC to maintain adequate uniaxial tensile properties. 1.75P-0.25R can be considered as the optimal mixture among all mixtures with hybrid fibres given its comparable uniaxial tensile properties, superior dynamic mechanical properties and improved sustainability to 2.0P-0R.

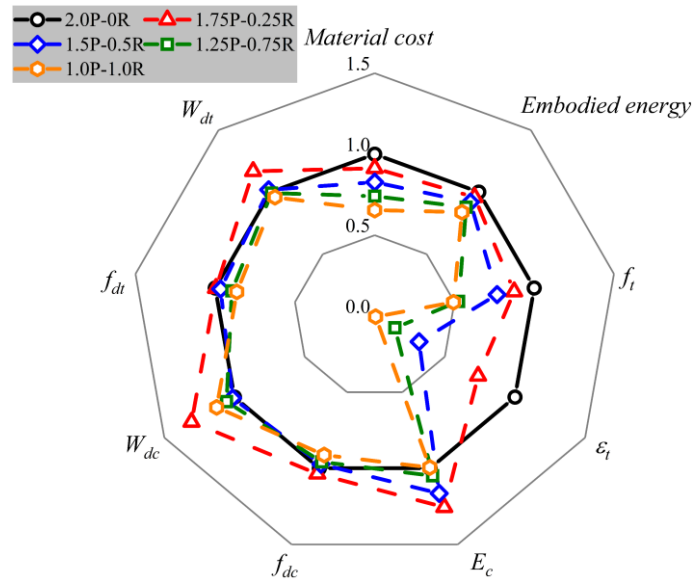


**Fig. 19.** A comparison between mono-PVA and hybrid PVA-RTP fibre reinforced EGC ( $f_t$  = uniaxial tensile strength,  $\varepsilon_t$  = tensile strain capacity,  $E_c$  = elastic modulus,  $f_{dc}$  = dynamic compressive strength,  $f_{dt}$  = dynamic splitting tensile strength,  $W_{dc}$  = energy absorption capacity under dynamic compression,  $W_{dt}$  = energy absorption capacity under dynamic splitting tension).

It was reported that 1.75P-0.25R exhibited a uniaxial tensile strength of 2.97 MPa and a strain capacity of 2.24%, while those for 2.0P-0R were 3.4 MPa and 3.04%, respectively ([Zhong and Zhang, 2021](#)). These properties can be strongly affected by the fibre distribution and internal pore structure of EGC ([Zhou et al., 2022](#)). [Fig. 20](#) presents the 3D pore structures of 2.0P-0R and 1.75P-0.25R and pore size distribution of them. It should be noted that only the pores with a diameter larger than 0.2 mm were considered here due to the limited resolution ([Lu et al., 2018a](#); [Xu et al., 2022](#)). As seen in [Figs. 20a](#) and [b](#), more than 99% of the pores in 2.0P-0R and 1.75P-0.25R had a size less than 0.1 mm<sup>3</sup> and reducing the PVA fibre content in EGC resulted in more fine pores. As seen in [Fig. 20c](#), although the percentages of pores with a diameter of 0.2-0.4 mm by the total number of pores for both mixtures were similar, the total volume of these pores for 1.75P-0.25R (4.66 mm<sup>3</sup>) was larger than that of 2.0P-0R (4.01 mm<sup>3</sup>). This can be attributed to the smaller aspect ratio of RTP fibres compared to PVA

fibres, which would introduce more air bubbles with smaller sizes whilst mixing. When the pore diameter was within 0.45-0.85 mm, the percentage of pores by the total number of pores and total volume for 2.0P-0R (4.84% and 2.24 mm<sup>3</sup>) were higher than those of 1.75P-0.25R (3.40% and 1.80 mm<sup>3</sup>), implying a larger probability of active flaw, which is defined as the flaw that can initiate the new crack when the tensile stress is lower than the bridging capacity of fibres (Xu et al., 2022). Additionally, the size of the largest pore in 2.0P-0R was bigger than that in 1.75P-0.25R. It was reported that the cracking is easier to be induced by the largest pore instead of a group of smaller pores (Lu et al., 2018a). These can explain why the multiple cracking behaviour of 2.0P-0R was more significant than that of 1.75P-0.25R, as indicated in a previous study (Zhong and Zhang, 2021). It is worth mentioning that the cracking behaviour of composites is not affected by the size of the pore but also its shape (Lu et al., 2018a). The total porosity by volume of the scanned block of 2.0P-0R and 1.75P-0.25R was 3.64% and 3.04%, respectively, which can support the previous discussion (Zhong and Zhang, 2021, 2022b) that the presence of PVA fibres can induce higher porosity inside the composites. This was also reported in Refs. (Liu et al., 2021; Long et al., 2021) that the addition of PVA fibres can entrap more air bubbles during the mixing process.

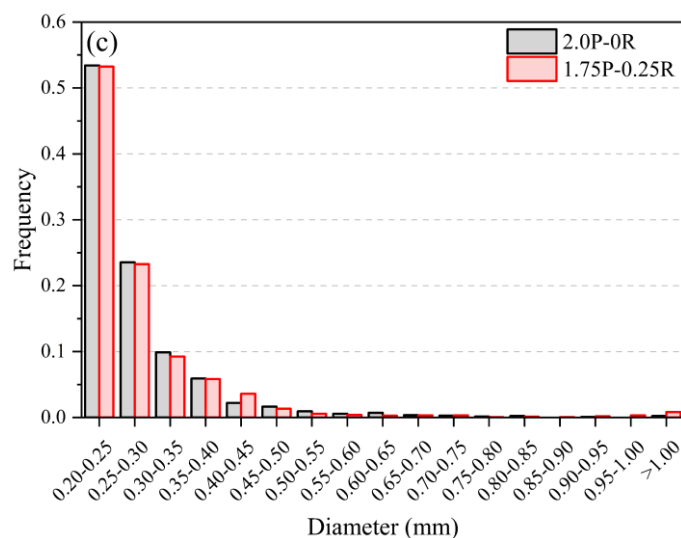
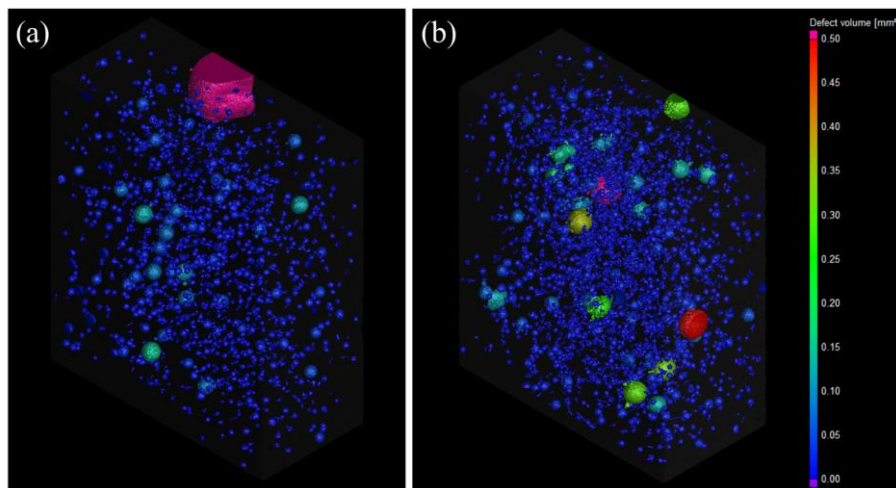


**Fig. 20.** 3D pore structures of (a) 2.0P-0R and (b) 1.75P-0.25R, and (c) pore size distribution of them obtained from XCT imaging.

On the other hand, the fibre bridging behaviour plays a dominant role when the crack appears during the uniaxial tension loading, which can be affected by fibre distribution and orientation. **Fig. 21** presents some XCT images of 2.0P-0R and 1.75P-0.25R, which reveal that fibres in both mixtures tended to be randomly distributed and orientated. The fibres distributed perpendicular to the loading direction are more effective in bridging the cracks and improving the ductility of composites. For 1.75P-0.25R, the incorporated RTP fibres can be easily pulled out during the crack propagation, which can lead to the ultimate failure of the sample before the appearance of the next crack. This explains the weaker tensile strain capacity observed in hybrid PVA-RTP fibre reinforced EGC compared to mono-PVA fibre reinforced EGC (see **Fig. 19**).

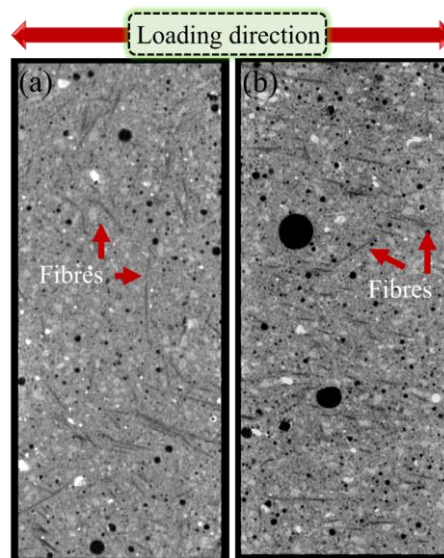


**Fig. 21.** Fibre distribution in EGC obtained from XCT: (a) 2.0P-0R, and (b) 1.75P-0.25R.

**Fig. 22** demonstrates the schematic failure mechanism of hybrid fibre reinforced EGC under dynamic splitting tension. Only one major splitting crack appears for hybrid fibre reinforced EGC after dynamic splitting tension, which is not pronounced at a lower strain rate. Meanwhile, many bridging fibres can be observed at the crack interface. As the strain rate rises, the crack width of the splitting crack becomes more extensive with noticeable triangular damage sections at two ends, where most fibres are pulled out or ruptured under this situation. Due to the synergistic fibre effect, smaller RTP fibre spacing, Stefan effect and pull-out behaviour of RTP fibre at different strain rates, the dynamic splitting tensile properties of hybrid fibre reinforced EGC can slightly surpass mono-PVA fibre reinforced EGC.

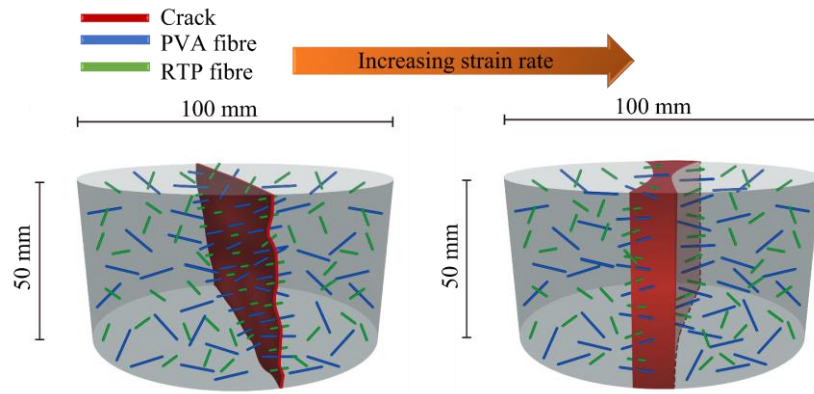


**Fig. 22.** Schematic failure mechanism of hybrid fibre reinforced EGC under dynamic splitting tension.

## 5. Conclusions

In this study, a series of tests were performed to investigate the effects of different fibres including polyvinyl alcohol (PVA) and recycled tyre polymer (RTP) fibres on the quasi-static and dynamic splitting tensile properties of engineered geopolymer composites (EGC). Based on the experimental results, the main conclusions can be listed as follows:

- Plain geopolymer exhibited extraordinarily brittle behaviour under quasi-static splitting tension, while the presence of PVA or RTP fibres improved the quasi-static tensile strength of geopolymers by 129.44-196.09% and maintained the structural integrity of samples. Increasing RTP fibre dosage in hybrid PVA-RTP fibre reinforced EGC led to a 3.36-18.40% reduction in quasi-static splitting tensile strength compared to EGC with 2.0% PVA fibre.
- The incorporation of PVA or RTP fibres significantly enhanced the dynamic splitting properties and reduced the damage level of geopolymers. The dynamic splitting tensile strength and energy absorption capacity of EGC were consistently improved with the increase of PVA fibre content, while replacing PVA fibre with 0.25-0.5% RTP fibre can slightly enhance the dynamic splitting tensile properties compared to EGC with 2.0% PVA fibre. The failure pattern, dynamic splitting tensile strength, dynamic increase factor and energy absorption capacity of all mixtures were strain-rate dependent, which can be well described using the proposed equations.
- More pulled out PVA fibres can be identified under dynamic loading due to the increased fibre properties with the change of strain rate, which is beneficial for the dynamic splitting tensile properties. Because of the inherent hydrophobic feature, the failure mode of RTP fibre did not change with strain rate, which can recompense for the loss of energy absorption induced by the ruptured PVA fibres but can impair the dynamic splitting tensile strength when the dosage of RTP fibre in EGC exceeded 0.5%.
- The utilisation of PVA fibres can induce higher porosity for EGC compared to RTP fibres. Considering the static and dynamic mechanical behaviour, cost-effectiveness, and sustainability,

the mixture incorporating 1.75% PVA fibre and 0.25% RTP fibre can be regarded as the optimal mixture for EGC.

- This study suggests that adopting 0.25-0.5% RTP fibre as a partial substitute for PVA fibre in EGC can lead to enhanced dynamic compressive and tensile properties, cost-effectiveness and sustainability of EGC, meanwhile retaining acceptable quasi-static mechanical properties.

### **Acknowledgements**

The authors gratefully acknowledge the financial support from the Engineering and Physical Sciences Research Council (EPSRC), UK under Grant No. EP/R041504/1 and the Royal Society, UK under Award No. IEC\NSFC\191417. The financial support provided by University College London (UCL) and China Scholarship Council (CSC) to the first author is gratefully acknowledged.

### **References**

- ASTM C496, 2017. Standard Test Method for Splitting Tensile Strength of Cylindrical Concrete Specimens. ASTM International, West Conshohocken, PA
- Bertholf, L.D., Karnes, C.H., 1975. Two-dimensional analysis of the split hopkinson pressure bar system. *Journal of the Mechanics and Physics of Solids* 23(1), 1-19.
- CEB-FIP model code 1990: Design code, 1990. Comite Euro-International Du Beton
- Chen, M., Chen, W., Zhong, H., Chi, D., Wang, Y., Zhang, M., 2019. Experimental study on dynamic compressive behaviour of recycled tyre polymer fibre reinforced concrete. *Cement and Concrete Composites* 98, 95-112.
- Chen, M., Zhong, H., Chen, L., Zhang, Y., Zhang, M., 2021. Engineering properties and sustainability assessment of recycled fibre reinforced rubberised cementitious composite. *Journal of Cleaner Production* 278, 123996.
- Chen, M., Zhong, H., Wang, H., Zhang, M., 2020. Behaviour of recycled tyre polymer fibre reinforced concrete under dynamic splitting tension. *Cement and Concrete Composites* 114, 103764.
- Chen, X., Ge, L., Zhou, J., Wu, S., 2017. Dynamic Brazilian test of concrete using split Hopkinson pressure bar. *Materials and Structures* 50(1).
- Chen, X., Wu, S., Zhou, J., 2014. Quantification of dynamic tensile behavior of cement-based materials. *Construction and Building Materials* 51, 15-23.
- Curosu, I., Mechtcherine, V., Millon, O., 2016. Effect of fiber properties and matrix composition on the tensile behavior of strain-hardening cement-based composites (SHCCs) subject to impact loading. *Cement and Concrete Research* 82, 23-35.
- Davidovits, J., 2002. Environmentally driven geopolymers cement applications, Proceedings of 2002 Geopolymer Conference. Melbourne, Australia.

Duxson, P., Provis, J.L., Lukey, G.C., van Deventer, J.S.J., 2007. The role of inorganic polymer technology in the development of 'green concrete'. *Cement and Concrete Research* 37(12), 1590-1597.

Farooq, M., Krishna, A., Banthia, N., 2022. Highly ductile fiber reinforced geopolymers under tensile impact. *Cement and Concrete Composites* 126, 104374.

FIB Model Code for Concrete Structures 2010, 2013. Comite Euro-International Du Beton

Hao, Y., Hao, H., 2016. Mechanical properties and behaviour of concrete reinforced with spiral-shaped steel fibres under dynamic splitting tension. *Magazine of Concrete Research* 68(21), 1110-1121.

Kan, L., Wang, F., Zhang, Z., Kabala, W., Zhao, Y., 2021. Mechanical properties of high ductile alkali-activated fiber reinforced composites with different curing ages. *Construction and Building Materials* 306, 124833.

Kanda, T., Li, V.C., 1998. Multiple cracking sequence and saturation in fiber reinforced cementitious composites. *Concrete Research and Technology* 9, 19-33.

Khan, M.I., Fares, G., Mourad, S., Abbass, W.J.J.o.M.i.C.E., 2016. Optimized Fresh and Hardened Properties of Strain-Hardening Cementitious Composites: Effect of Sand Size and Workability. *Journal of Materials in Civil Engineering* 28(12), 04016152.

Khan, M.Z.N., Hao, Y., Hao, H., Shaikh, F.U.A., 2018. Experimental evaluation of quasi-static and dynamic compressive properties of ambient-cured high-strength plain and fiber reinforced geopolymer composites. *Construction and Building Materials* 166, 482-499.

Khan, M.Z.N., Hao, Y., Hao, H., Shaikh, F.u.A., 2019. Mechanical properties and behaviour of high-strength plain and hybrid-fiber reinforced geopolymer composites under dynamic splitting tension. *Cement and Concrete Composites* 104, 103343.

Lai, D., Demartino, C., Xiao, Y., 2022. High-strain rate tension behavior of Fiber-Reinforced Rubberized Concrete. *Cement and Concrete Composites* 131, 104554.

Lee, Y., Choi, J.-I., Kim, H.-K., Lee, B.Y., 2017. Effects of a defoamer on the compressive strength and tensile behavior of alkali-activated slag-based cementless composite reinforced by polyethylene fiber. *Composite Structures* 172, 166-172.

Li, V.C., 2019. *Engineered Cementitious Composites (ECC): Bendable Concrete for Sustainable and Resilient Infrastructure*. Springer.

Li, X., Zhang, Y., Shi, C., Chen, X., 2020. Experimental and numerical study on tensile strength and failure pattern of high performance steel fiber reinforced concrete under dynamic splitting tension. *Construction and Building Materials* 259, 119796.

Liu, F., Xu, K., Ding, W., Qiao, Y., Wang, L., 2021. Microstructural characteristics and their impact on mechanical properties of steel-PVA fiber reinforced concrete. *Cement and Concrete Composites* 123, 104196.

Long, W.-J., Li, H.-D., Mei, L., Li, W., Xing, F., Khayat, K.H., 2021. Damping characteristics of PVA fiber-reinforced cementitious composite containing high-volume fly ash under frequency-temperature coupling effects. *Cement and Concrete Composites* 118, 103911.

Lu, C., Li, V.C., Leung, C.K.Y., 2018a. Flaw characterization and correlation with cracking strength in Engineered Cementitious Composites (ECC). *Cement and Concrete Research* 107, 64-74.

Lu, C., Yu, J., Leung, C.K.Y., 2018b. Tensile performance and impact resistance of Strain Hardening Cementitious Composites (SHCC) with recycled fibers. *Construction and Building Materials* 171, 566-576.

Lyu, B.-C., Ding, C., Guo, L.-P., Chen, B., Wang, A.-g., 2021. Basic performances and potential research problems of strain hardening geopolymer composites: A critical review. *Construction and Building Materials* 287, 123030.

Malvar, L.J., Ross, C.A., 1998. Review of strain rate effects for concrete in tension. *ACI Mater. J.* 95, 735-739.

Maruta, M., 2005. New high-rise RC structure using pre-cast ECC coupling beam. *Concrete Journal* 43(11), 18-26.

Merli, R., Preziosi, M., Acampora, A., Lucchetti, M.C., Petrucci, E., 2019. Recycled fibers in reinforced concrete: A systematic literature review. *Journal of Cleaner Production* 248, 119207.

Nematollahi, B., Sanjayan, J., Qiu, J., Yang, E.-H., 2017a. High ductile behavior of a polyethylene fiber-reinforced one-part geopolymer composite: A micromechanics-based investigation. *Archives of Civil and Mechanical Engineering* 17(3), 555-563.

Nematollahi, B., Sanjayan, J., Qiu, J., Yang, E.-H., 2017b. Micromechanics-based investigation of a sustainable ambient temperature cured one-part strain hardening geopolymer composite. *Construction and Building Materials* 131, 552-563.

Nematollahi, B., Sanjayan, J., Shaikh, F.U.A., 2014. Comparative deflection hardening behavior of short fiber reinforced geopolymer composites. *Construction and Building Materials* 70, 54-64.

Nguyễn, H.H., Luong, Q.-H., Choi, J.-I., Ranade, R., Li, V.C., Lee, B.Y., 2021. Ultra-ductile behavior of fly ash-based engineered geopolymer composites with a tensile strain capacity up to 13.7%. *Cement and Concrete Composites* 122, 104133.

Onuaguluchi, O., Banthia, N., 2017. Durability performance of polymeric scrap tire fibers and its reinforced cement mortar. *Materials and Structures* 50, 158.

Trindade, A.C.C., Heravi, A.A., Curosu, I., Liebscher, M., de Andrade Silva, F., Mechtcherine, V., 2020. Tensile behavior of strain-hardening geopolymer composites (SHGC) under impact loading. *Cement and Concrete Composites* 113, 103703.

Van den Heede, P., Mignon, A., Habert, G., De Belie, N., 2018. Cradle-to-gate life cycle assessment of self-healing engineered cementitious composite with in-house developed (semi-)synthetic superabsorbent polymers. *Cement and Concrete Composites* 94, 166-180.

Chen, W., Song, B., 2011. *Split Hopkinson (Kolsky) Bar: Design, Testing and Applications*. Springer.

Wang, S., Zhang, M.-H., Quek, S.T., 2011. Effect of high strain rate loading on compressive behaviour of fibre-reinforced high-strength concrete. *63(11)*, 813-827.

Wang, Y., Chan, C.L., Leong, S.H., Zhang, M., 2020. Engineering properties of strain hardening geopolymer composites with hybrid polyvinyl alcohol and recycled steel fibres. *Construction and Building Materials* 261, 120585.

Wang, Y., Wang, Y., Zhang, M., 2021. Effect of sand content on engineering properties of fly ash-slag based strain hardening geopolymer composites. *Journal of Building Engineering* 34, 101951.

Wang, Y., Zhong, H., Zhang, M., 2022. Experimental study on static and dynamic properties of fly ash-slag based strain hardening geopolymer composites. *Cement and Concrete Composites* 129, 104481.

Wu, M., Qin, C., Zhang, C., 2014. High strain rate splitting tensile tests of concrete and numerical simulation by mesoscale particle elements. *Journal of Materials in Civil Engineering* 26(1), 71-82.

Wu, S., Chen, X., Zhou, J., 2012. Tensile strength of concrete under static and intermediate strain rates: Correlated results from different testing methods. *Nucl. Eng. Des.* 250, 173-183.

Wu, Z., Shi, C., He, W., Wang, D., 2017. Static and dynamic compressive properties of ultra-high performance concrete (UHPC) with hybrid steel fiber reinforcements. *Cement and Concrete Composites* 79, 148-157.

Xu, L.-Y., Huang, B.-T., Li, V.C., Dai, J.-G., 2022. High-strength high-ductility Engineered/Strain-Hardening Cementitious Composites (ECC/SHCC) incorporating geopolymer fine aggregates. *Cement and Concrete Composites* 125, 104296.

Yang, E.-H., Li, V.C., 2014. Strain-rate effects on the tensile behavior of strain-hardening cementitious composites. *Construction and Building Materials* 52, 96-104.

Yoo, D.-Y., Bantia, N., 2019. Impact resistance of fiber-reinforced concrete – A review. *Cement and Concrete Composites* 104, 103389.

Yu, J., Leung, C.K., 2017. Strength improvement of strain-hardening cementitious composites with ultrahigh-volume fly ash. *Journal of Materials in Civil Engineering* 29, 05017003.

- Yu, J., Yao, J., Lin, X., Li, H., Lam, J.Y.K., Leung, C.K.Y., Sham, I.M.L., Shih, K., 2018. Tensile performance of sustainable Strain-Hardening Cementitious Composites with hybrid PVA and recycled PET fibers. *Cement and Concrete Research* 107, 110-123.
- Zeng, Q., Wang, X., Yang, P., Wang, J., Zhou, C., 2019. Tracing mercury entrapment in porous cement paste after mercury intrusion test by X-ray computed tomography and implications for pore structure characterization. *Mater. Charact.* 151, 203-215.
- Zhang, D., Tan, K.H., 2020. Effect of various polymer fibers on spalling mitigation of ultra-high performance concrete at high temperature. *Cement and Concrete Composites* 114, 103815.
- Zhang, D., Yu, J., Wu, H., Jaworska, B., Ellis, B.R., Li, V.C., 2020. Discontinuous micro-fibers as intrinsic reinforcement for ductile Engineered Cementitious Composites (ECC). *Composites Part B: Engineering* 184, 107741.
- Zhang, S., Li, V.C., Ye, G., 2020. Micromechanics-guided development of a slag/fly ash-based strain-hardening geopolymer composite. *Cement and Concrete Composites* 109, 103510.
- Zhang, S., Li, Z., Ghiassi, B., Yin, S., Ye, G., 2021. Fracture properties and microstructure formation of hardened alkali-activated slag/fly ash pastes. *Cement and Concrete Research* 144, 106447.
- Zhao, X., Li, Q., Xu, S., 2020. Contribution of steel fiber on the dynamic tensile properties of hybrid fiber ultra high toughness cementitious composites using Brazilian test. *Construction and Building Materials* 246, 118416.
- Zhao, Y., Shi, T., Cao, L., Kan, L., Wu, M., 2021. Influence of steel slag on the properties of alkali-activated fly ash and blast-furnace slag based fiber reinforced composites. *Cement and Concrete Composites* 116, 103875.
- Zhong, H., Zhang, M., 2021. Effect of recycled tyre polymer fibre on engineering properties of sustainable strain hardening geopolymer composites. *Cement and Concrete Composites* 122, 104167.
- Zhong, H., Zhang, M., 2022a. 3D printing geopolymers: A review. *Cement and Concrete Composites* 128, 104455.
- Zhong, H., Zhang, M., 2022b. Effect of recycled polymer fibre on dynamic compressive behaviour of engineered geopolymer composites. *Ceramics International* 48(16), 1151-1168.
- Zhou, W., Zhang, Y., Ma, L., Li, V.C., 2022. Influence of printing parameters on 3D printing engineered cementitious composites (3DP-ECC). *Cement and Concrete Composites* 130, 104562.